NOVEL METHODS FOR AUTOMATIC SEGMENTATION OF ABNORMAL LUNG PARENCHYMA UTILIZING WATERSHED AND WAVELET TRANSFORMS

by

Rushin Shojaii
BASc, Iran University of Science and Technology, Tehran, Iran, 1993

A thesis
presented to Ryerson University
in partial fulfillment of the
requirement for the degree of
Master of Applied Science
in the Program of
Electrical and Computer Engineering.

Toronto, Ontario, Canada, 2006

Author's Declaration

I hereby declare that I am the sole author of this thesis.
I authorize Ryerson University to lend this thesis to other institutions or individuals for the purpose of scholarly research.
Signature

I further authorize Ryerson University to reproduce this thesis by photocopying or by other means, in total or in part, at the request of other institutions or individuals for the purpose of scholarly research.
Signature

Instructions on Borrowers

Ryerson University requires the signatures of all persons using or photocopying this thesis. Please sign below, and give address and date.

Abstract

Rushin Shojaii, "Novel Methods for Automatic Segmentation of Abnormal Lung Parenchyma Utilizing Watershed and Wavelet Transforms", MASc, Electrical and Computer Engineering, Ryerson University, Toronto, 2006

CT scan of the thorax is widely used to diagnose and evaluate numerous lung diseases. These scans yield a large amount of image data. The expanding volume of thoracic CT studies along with the increase of image data, elucidates the need of computer-aided diagnosis (CAD) schemes to assist the radiologists. Since several lung diseases are diagnosed based on the patterns of lung tissue in medical images, texture segmentation is an essential part of the most CAD systems.

The preprocessing step of most CAD systems is lung segmentation. In the first part of this thesis a novel approach for lung segmentation is proposed. The proposed method is based on watershed transform, which is fast and accurate. Lung region is precisely marked with internal and external markers. The markers are combined with the gradient image of the original data, then watershed transform is applied on the combined data to find the lung borders. A "Rolling ball" filter is used to fill the cavities and make the contour smooth while preserving the original borders.

In the second part of this research work a novel composite method is proposed to segment the abnormality in lung tissue. The proposed approach is based on wavelet transform and intensity similarities. Our focus is on the honeycomb texture in lung tissue, which occurs with several interstitial lung diseases. After segmenting lung regions, Wavelet Transform is applied to decompose the image. The transformed lung region is thresholded to extract high resolution areas. Then the regions with low pixel intensities are kept and grown to segment the honeycomb regions. The proposed method has been tested on 91 pediatric chest CT images containing healthy and unhealthy lung images. Statistical analysis has been done and the results show the sensitivity of 100% along with the average Specificity of 95.14%. A comparison with AMFM (82.5% sensitivity and 99.9% specificity)and ANN methods (100% sensitivity and 88.1% specificity) reveals the superiority of the proposed approach.

The test results of both the lung segmentation and abnormal lung tissue segmentation techniques validate the robustness of the proposed methods.

Acknowledgments

I would like to express my sincere appreciation to my advisor, Dr. Javad Alirezaie for his kind help, guidance, support and encouragement throughout my study. It is also a great pleasure to acknowledge the assistance I have received from Dr. Paul Babyn from the Hospital for Sick Children. He provided me with paediatric CT images along with his valuable technical advices. I am grateful to the professors in Ryerson University who gave me confidence as well as instruction. I would also like to thank Ms. Dawn Wright, Graduate Program Administrator of Electrical and Computer Engineering, who always helped me generously. My friends, Taraneh and Alen, are greatly acknowledged for their proofreading assistance.

I am grateful to my lab mates and dear friends, who were so helpful and made a great professional environment to develop researches.

I would like to thank my beloved husband, Ali, for his unbelievable support and encouragement through my entire study. Many thanks to my lovely parents and my dearest sister who are always my inspirations.

And, I would like to dedicate my thesis to my husband and my newborn baby, Pedram, who are the hopes of my life.

Contents

1 Introduction 1
- 1.1 Computer-Aided Diagnosis . . . 2
- 1.2 Pulmonary Anatomy . . . 2
- 1.3 Computed Tomography of Lung . . . 3
  - 1.3.1 Healthy Lung . . . 4
  - 1.3.2 Abnormal Lung . . . 5
- 1.4 Image Segmentation . . . 6
- 1.5 Texture and Texture Analysis . . . 7
- 1.6 Contribution . . . 8

2 Literature Review 10
- 2.1 Lung Segmentation . . . 10
  - 2.1.1 Anatomical Model . . . 10
  - 2.1.2 Optimal Threshold . . . 11
  - 2.1.3 Histogram Tresholding . . . 12
- 2.2 Texture Segmentation . . . 14
  - 2.2.1 Previous Works . . . 16

3 Methodology 18
- 3.1 Lung Segmentation . . . 18
  - 3.1.1 Watershed Transform . . . 18
  - 3.1.2 Gradient Image (Step 1) . . . 21
  - 3.1.3 Internal Marker (Step 2) . . . 21
  - 3.1.4 External Marker (Step 3) . . . 23
  - 3.1.5 Imposing Regional Minima (Step 4) . . . 23
  - 3.1.6 Watershed Transform (Step 5) . . . 24
  - 3.1.7 Smoothing and Filling the Cavities (Step 6) . . . 25
- 3.2 Honeycomb Lung Segmentation using Entropy Filtering . . . 25
  - 3.2.1 Spectral Measures . . . 26
  - 3.2.2 Statistical Measures . . . 27
  - 3.2.3 Entropy Filter . . . 30
  - 3.2.4 Extracting Honeycomb from other Textures . . . 32

3.3 Honeycomb Lung Segmentation using Wavelet Transform 34
3.3.1 Wavelet Transform 35
3.3.2 Histogram Thresholding 38
3.3.3 Extracting Honeycomb from other Textures 38

4 Validation **42**
4.1 Lung Segmentation Verification 43
4.1.1 Experimental Results 43
4.1.2 A Comparison 43
4.2 Abnormal Lung Tissue Segmentation 46

5 Conclusions and Future Works **50**
5.1 Conclusion 51
5.2 Future Works 52

A The Anatomy of Lung **54**
A.1 Lung Tissue Abnormalities 55
A.1.1 Emphysema 55

B Fundamentals of Computed Tomography **57**
B.1 Helical/Spiral Computed Tomography 59
B.1.1 Hounsfield Unit 60
B.1.2 Digital Imaging and Communications in Medicine (DICOM) Standard 61

List of Figures

1.1 Human respiratory system [1]. 3
1.2 CT images of different parts of chest. 4
1.3 CT image of healthy lung. 5
1.4 Some examples of abnormal lung CT images [2]. 7

3.1 Watershed Lines and Catchment Basins (Courtesy of Steve Eddins). 19
3.2 The process of building Watershed Lines (Courtesy of Tesi di Laurea). 21
3.3 (a) Original pulmonary CT image. (b) The gradient image of figure (a) using Sobel masking. (c) Result with oversegmentation obtained using standard watershed transform on the gradient image. 22
3.4 (a) Internal Marker (b) External Marker. 24
3.5 (a) Imposed regional minima in the marked area. (b) Segmented lung contour. 24
3.6 (a) Smoothed lung contour using rolling ball filter (b) Segmented lung regions. 25
3.7 Two lung CT images with honeycombing [2]. 26
3.8 Healthy, Honeycomb and tissue with vessel branches. 27
3.9 : Left: S(r) Right: $S(\theta)$ of healthy, honeycomb and area with vessel branches. 28
3.10 $S(r, \theta)$ of healthy, honeycomb and nodular. 29
3.11 CT image of Honeycomb Lung. 31
3.12 Entropy filtered image. 31
3.13 Thresholded filtered image. 32
3.14 Original gray scale pixel values of thresholded image. 32
3.15 Darkest areas of the thresholded image. 33
3.16 Seeds. 33
3.17 The mask used for region growing. 34
3.18 The mask for honeycomb area. 34
3.19 Extracted honeycomb tissue of the lung. 35
3.20 Wavelet Transform. 37
3.21 High resolution regions. 38
3.22 Masking high resolutions areas on original image. 38
3.23 a) Seed or marker, b) Mask. 39
3.24 a) Result of region growing, b) Lung with honeycombing, c) Segmented honeycomb area. 40
3.25 a) Original slice with honeycoming, b) Segmented honeycomb area. 40

3.26 Graphical User Interface which is developed to test the proposed algorithms. 41

4.1 Left: Original CT images. Right: Segmented lung Regions. 44
4.2 (a) Originl pulmonary CT image. (b) Segmented lung borders. (c) Smoothed lung borders. (d) Lung regions. 45
4.3 First row: Original Chest CT Image. Second Row: Segmented Lung with Watershed Transform. Third Row: Segmented Lung with Optimal Thresholding. 49

A.1 Lung and its Parenchyma [1]. 56

B.1 A Modern CT scanner (Extracted from Aquilion64 User's Guide. 58
B.2 Fundamentals of a CT scanner (Extracted from Imaginis the Breast Cancer Resource). 59
B.3 Schematic drawing of the spiral CT [3]. 60
B.4 Schematic of interpolation rationale for helical CT [3]. 61

List of Tables

3.1 Statistical Measures of Three Lung Different Tissue 30

4.1 Datasets Specifications 47
4.2 Statistical Analysis of the Composite Method 47

Chapter 1

Introduction

Recent advances in Computed Tomography (CT) technology has enabled it to be widely used in diagnosing and quantifying different diseases. In particular, the expanding volume of thoracic CT studies along with the increase of image data, elucidates the need for Computer Aided Diagnosis (CAD) schemes to assist the radiologists [4].

The first step of most CAD systems is lung segmentation. Several lung diseases are diagnosed by investigating the patterns of lung tissue in pulmonary CT images, therefore texture segmentation and analysis is another important part of CAD systems.

In the first part of this thesis a novel approach to segment lung regions in CT images is proposed, developed and tested. In the second part a new composite method, which is composed of a multi resolution technique and the methods based on intensity similarities of the regions, is proposed to detect the lung tissue abnormalities.

In order to differentiate between normal and abnormal lung images, it is essential to understand the different aspects of lung CT images and various textures in lung tissues. In this chapter, first CAD systems are briefly discussed, then the respiratory system is reviewed. The fundamentals of chest CT is discussed in section 1.3. In sections 1.3.1 and 1.3.2 several lung CT images including healthy and unhealthy lung tissue are shown. These images compare various textures that might exist in an unhealthy lung. A brief knowledge about object and texture segmentation and analysis is given in sections 1.4 and 1.5. The contribution of this thesis and its outline are discussed in the last section.

1.1 Computer-Aided Diagnosis

While computer technology has had a tremendous impact on medical imaging, the interpretation of medical images is still best performed by humans. During the coming decades, the use of computers in image interpretation is expected to increase and improve dramatically [4]. Already Computer-Aided Diagnosis (CAD) has been described as "a second pair of eyes for the radiologist" [4], and in some cases computer algorithms are outperforming human observers.

Methodological researchers currently focus on segmentation and feature extraction approaches and techniques for pattern recognition. The application areas are chest, brain, heart, blood vessels, bone and all other parts of the body which can be examined through medical images.

The focus of this research is on lung and texture segmentation to evaluate lung tissue in pulmonary (chest) CT images. The main motivation behind this research is to improve the CAD systems which are used to locate abnormal lung tissue without massive invasion.

1.2 Pulmonary Anatomy

Lungs are the central organs of the human respiratory system. Other organs of the pulmonary system include the nose, mouth, rib cage and diaphragm which are diagramatically shown in figure 1.1. The main function of the respiratory system is to transport oxygen from the atmosphere into the lung tissues to support cellular metabolism, and to transport carbon dioxide from the lung tissues out to the atmosphere. The pulmonary system includes lungs and the respiratory airways leading into the lungs and the structures of the thorax involved in producing the movement of air through the airways into and out of the lungs [1]. For more details on lung anatomy please refer to appendix A.

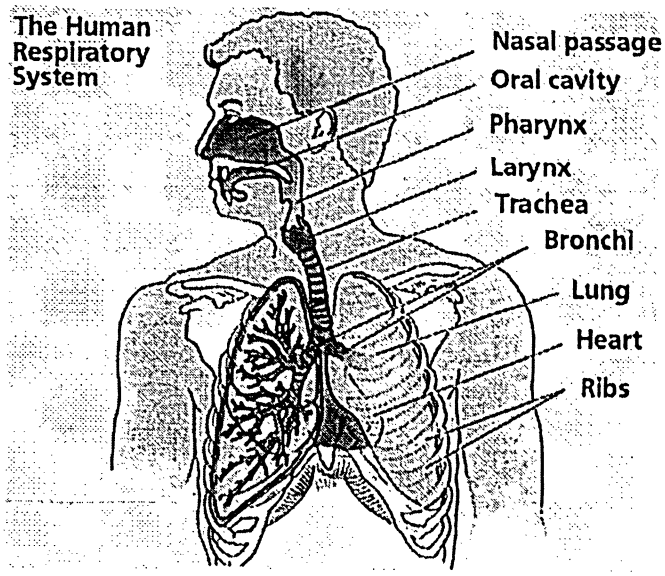

Figure 1.1: Human respiratory system [1].

1.3 Computed Tomography of Lung

Recent advances in multi-slice CT technology have enabled the acquisition of high spatial volumetric pulmonary images within a breath hold. The fundamentals of CT scanners along with Helical CT ones are described in Appendix B and B.1. CT images of lungs have been widely used to study interstitial lung diseases. A lung CT dataset consists of an abundance of cross-sectional images (slices) from different parts of the lung with a specified distance (thickness) between them. As it is shown in figure 1.2, images from the upper part of the chest (figure 1.2-a) may contain just the trachea and small parts of the lung and as it goes down to the lower parts of the chest (figure 1.2-b), lung regions will be evident. In the lower parts of the chest (figure 1.2-c) diaphragm will be seen along with the small parts of the lung.

A standardized scale named Hounsfield Unit is used to facilitate the intercomparison of CT values obtained from different CT scanners (Appendix B.1.1). In pulmonary CT images the air will appear with a mean intensity of approximately -1000 Hounsfield Units (HU), the

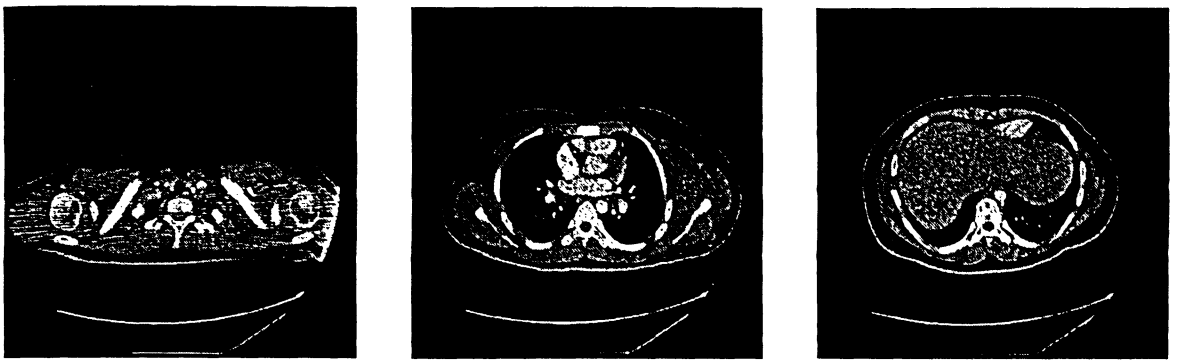

(a) Upper part of chest (b) Middle part of chest (c) Lower part of chest

Figure 1.2: CT images of different parts of chest.

lung region will be in the range of [-1000 to -400] HU, and the chest wall, blood and bone will be much more dense and well above -400 HU.

The format of the pulmonary CT images used for this research is DICOM (Appendix B.1.2). DICOM is a cooperative standard and its goal is to achieve compatibility and improvement in workflow efficiency between imaging systems. The metadata in a DICOM file provides information, such as the size, dimensions, and bit depth of the image. In addition, the DICOM specification defines numerous other metadata fields that describe many other characteristics of the data, such as the modality used to create the data, the equipment settings used to capture the image, and information about the study.

1.3.1 Healthy Lung

In order to interpret lung CT images, it is required to have a detailed understanding of normal lung anatomy and of the pathologic alterations, which occur in the presence of disease. Figure 1.3 shows a CT image of a healthy lung. The background of the lung area is almost uniform with insignificant changes in intensity. Vessel and artery branches can be clearly seen in the image. Since vessels contain blood which is denser than air they look brighter than the lung tissue in the image. Pulmonary airways also can be seen in lung images especially in High Resolution Computed Tomography (HRCT). Since these airways are filled with air, the cross-section view of them happens to be seen in CT images as an

Figure 1.3: CT image of healthy lung.

empty circle. Whereas the cross-section of blood vessels can be seen as filled circles [2].

1.3.2 Abnormal Lung

The detection and diagnosis of diffuse lung disease using high-resolution computed tomography (HRCT) is based on the recognition of specific abnormal findings. In this section it is shown that different lung diseases cause different patterns in lung tissue. Radiologists study these patterns to diagnose any abnormality of the lung to monitor the improvement of the disease during the healing process.

The patterns of lung abnormalities vary based on the disease syndromes. For example figure 1.4 shows four different examples of abnormal lung tissue. Figure 1.4-a shows an emphysematous lung. Since emphysema is an interstitial lung disease (Appendix A.1.1), it affects pixels' density such that the emphysematous regions in the images appear darker (with lower density) [2].

In patients with bronchiectasis, the abnormal thick-walled and dilated bronchi often appear much larger than the adjacent pulmonary artery branches (figure1.4-b). This results in the appearance of large ring shadows, each associated with a small rounded capacity. This is considered to be diagnostic of bronchiectasis [2].

Figure 1.4-c shows a lung with hematogenous metastases from a rectal carcinoma. Multiple

small, well-defined nodules are visible with involvement of peripheral pleural surfaces. The overall pattern of distribution is random.

The honeycomb lung is composed of a porous network of fibrous walled cysts (figure 1.4-d), which resembles a beehive or, more characteristically, a sponge. The cysts are filled with air, which makes them look like dark holes in CT images. Honeycombing can be the result of a variety of lung diseases including Idiopathic pulmonary fibrosis (IPF), asbestosis, histiocytosis, sarcoidosis, chronic hypersensitivity pneumonitis and rheumatologic diseases [2]. In other words honeycombing is a feature from which several interstitial diseases could be diagnosed.

These patterns are some examples of various patterns that might occur in case of a diseased lung.

Studying these patterns implies that by utilizing texture segmentation techniques, patterns in Computer Aided Diagnosis (CAD) can classify abnormal lung CT images from healthy ones. Furthermore, quantitative analysis of these textures will be a useful tool to help a radiologist to study the improvement of a disease during a healing process.

1.4 Image Segmentation

The subdivision of an image into components such as points, lines, or regions is called image segmentation. The process is based on local similarities in pixels' intensities. Image segmentation is a prerequisite for processes such as computer-aided diagnosis, quantitative analysis, visualization, registration and atlas-matching.

Generally, image segmentation algorithms are based on one of the two properties of intensity values: discontinuity and similarity [5]. In the first category the approach is to partition an image based on abrupt changes in intensity, such as edges. The main approaches in the second category, are based on partitioning an image into regions that are similar according to a set of predefined criteria. Thresholding, region growing, and region splitting and merging are examples of methods in this category.

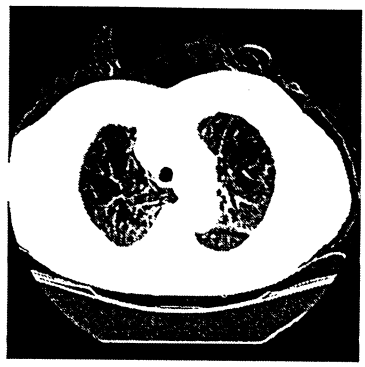

(a) Emphysema

(b) Bronchiactesis

(c) Nodular(Hematogenous metastases)

(d) Honeycomb Lung

Figure 1.4: Some examples of abnormal lung CT images [2].

1.5 Texture and Texture Analysis

Textures in general, are complex visual patterns composed of entities, or subpatterns, that have characteristics like brightness, color, size, etc. Thus texture can be considered as a group of similarities in an image [6]. The properties of local subpatterns give rise to the perceived lightness, uniformity, density, roughness, regularity, linearity, frequency, phase, directionality, coarseness, randomness, fineness, smoothness, granulation etc. [7]. Texture analysis has four major issues:

- Feature extraction: to compute characteristics of an image which are able to describe its texture properties numerically.
- Texture discrimination: to partition a textured image into regions, each corresponding to a perceptually homogeneous texture (leads to image segmentation).

- Texture classification: to determine to which physically defined classes (such as normal and abnormal tissue) a homogeneous texture region belongs.
- Object shape determination: to reconstruct 3D surface geometry from texture information.

Feature extraction is the first stage of image texture analysis. Results obtained from this stage are used for texture discrimination, texture classification or object shape determination. The second part of this research is confined mainly to feature extraction, texture discrimination, and texture classification of lung tissue.

1.6 Contribution

The goal of this thesis is to distinguish healthy pulmonary chest CT images from unhealthy ones based on the existing textures of lung tissue, which show the abnormalities.
A novel approach is proposed and developed to segment lung regions from lung CT images. Marker-based watershed transform has been utilized to accomplish this task. Despite its simplicity, this method is highly robust, accurate, and fast.
In order to segment suspicious regions of lung tissue a new composite algorithm has been utilized. The technique is based on multi-resolution methods using wavelet transform combined with intensity similarities.
To segment abnormal textures in CT images entropy filtering has been implemented and compared to the proposed algorithm.
The thesis is organized as follows:
Chapter 2 gives a brief background over the concepts of segmentation methods and the previous works for lung and texture segmentation in lung CT images. It also discusses the existing feature extraction and classification methods.
Chapter 3 explains the utilized methods in this research including lung segmentation and texture segmentation.
Chapter 4 contains the experimental and analytical results and demonstrates the accuracy

of the methods utilized.

Chapter 5 is dedicated to conclusion and potential future works.

Chapter 2

Literature Review

This chapter explains previous works on lung segmentation. It also reviews the existing methods of texture discrimination and analysis of lung tissue which have been utilized by other researchers to detect lung abnormalities.

2.1 Lung Segmentation

To provide useful and reliable information, most CAD methods require identification of the lung boundaries within the images, a preprocessing step known as "lung segmentation". Limiting further processing to the lungs greatly reduces computation time and memory, because the lung occupies a fraction of the total volume of data. So, lower amount of memory is required during the computation time. Automated lung segmentation is also useful for image data visualization. Three dimensional display of CT image data is an area of rapid development. Lung segmentation must be accurate because abnormalities such as lung nodules may exist at the extreme periphery of the lungs. If the entire lung is not segmented, such abnormalities will be lost in subsequent analysis. In this chapter, the previous works from other researchers are reviewed.

2.1.1 Anatomical Model

Brown *et al.* [8] developed a knowledge-based, automated method for segmenting volumetric chest CT datasets. The method utilizes a modular architecture consisting of an anatomical

model, image processing routines, and an inference engine, the interactions of which are governed by a blackboard [9].

The principle of operation is as follows: for each modeled object, constraints on features are derived and written to the blackboard. Image processing routines write corresponding feature representations of segmented image primitives to the blackboard. The inference engine reads the data from both sources and does the matching. Its conclusions are then also written back to the blackboard and the information can be used to guide further matching. The mapping to feature space allows the model and image data representations to be independent. They initially modeled the chest wall and mediastinum, central tracheobronchial tree, and right and left lungs in terms of attenuation threshold, shape, contiguity, volume, and relative position.

One of the drawbacks of this method is its complexity in implementation. It is also dependent on a priory knowledge of the structure of the lung while lung can have various shapes and lung tissue have different patterns.

2.1.2 Optimal Threshold

Hu *et al.* [5], [10], [11] have utilized optimal thresholding to segment lung regions instead of fixed threshold. Connectivity and topological analysis are used to further refine regions that represent the extracted lungs.

It is assumed that the image volume contains only two types of voxels: 1) voxels within the very dense body and chest wall structures (the body voxels) and 2) low-density voxels in the lungs or in the air surrounding the body of the subject (the nonbody voxels). Optimal thresholding is utilized to select a segmentation threshold to separate the body from the nonbody voxels, and then identify the lungs as the low-density cavities inside of the body.

After applying the optimal threshold, the nonbody voxels will correspond to the air surrounding the body, the lungs, and other low-density regions within the image volume (i.e., gas in the bowel). Three-Dimensional connected components labeling is used to identify the lung voxels. The background air is eliminated by deleting regions that are connected to the

border of the image. Small, disconnected regions are discarded if the region volume is too small. To identify the lungs, the two largest components in the volume are retained, with the additional constraint that each component must be larger than a predetermined minimum volume. Only the components with a volume greater than one percent of the total image voxel count are retained.

The high-density vessels in the lung will be labeled as body voxels during the optimal thresholding step. As a result, the 3-D lung regions will contain unwanted interior cavities. Topological analysis, similar to that used in [12] is used to fill the lung regions and eliminate the interior cavities.

Segmentation of the Large Airways: To perform quantitative analysis on the lung tissue, the trachea and large airways must be identified and separated from the left and right lungs.

The trachea and left and right mainstem bronchi are identified in the original gray-level image data using a closed-space dilation with a unit radius kernel [13]. This procedure is equivalent to the directed slice-by-slice region growing. To initialize the closed-spaced dilation, the location of the trachea is automatically identified by searching for the large, circular, air-filled region near the center of the first few slices in the data set. Regions in the current slice provide potential seed point positions for the next slice. The slice-by-slice growing procedure is stopped when the size of the region on a new slice increases dramatically, indicating that the airways have merged into the low-density lung tissue.

Optimal thresholding is a heuristic approach, so, it is time consuming and as it is shown in chapter 4, it is not successful in segmenting lungs with some abnormalities including honeycombing. The trachea elimination for each slice is dependent on the previous slice, while it can simply be done on each slice independently.

2.1.3 Histogram Tresholding

Armato *et al.* utilized histogram thresholding to segment lung regions ([14],[15]). A cumulative gray-level profile is constructed from pixels along a diagonal of the CT section image, and the shape of this profile is used to identify a gray-level threshold. A binary image is

created by thresholding the section image. An eight-connected border tracking algorithm [11] is used to identify the outer margin of the largest object in the binary image, and the set of pixels in the original image that lie within this contour is considered the segmented thorax region. The presence of a single, large lung segmentation region in any section indicates that gray-level thresholding has fused the two lung regions at the anterior junction ([8],[10],[16],[17]). Distinction between left and right lungs is often required for more detailed image analysis. Consequently, the single lung region is separated into two regions by eliminating pixels along the anterior junction line. The most anterior point along the cardiac aspect of the lung region is identified. Because the anterior junction line typically demonstrates a mild curvature, a search of 10 pixels on either side of the initial anterior junction line is performed in each image row intercepted by the initial anterior junction line to locate the local maximum. This set of local maximum pixels represents the anterior junction line, which is turned "off" in the lung region to create two distinct regions from what had been erroneously identified by initial gray-level thresholding as a single segmented lung region.
Gray-level thresholding tends to include the trachea and main bronchi within the segmented lung regions [16]. To ensure that these structures are not subsequently included in the segmented lung regions, the trachea and main bronchi are eliminated from the segmented thorax regions in all sections in which they appear. A seed point for trachea segmentation is automatically identified in the superiormost CT section. This seed point is the pixel with the lowest gray level in a region about the center-of-mass of the thorax and is assumed to exist within the trachea. Region-growing technique [11] is used to expand the identified trachea region about the seed point; as the graylevel threshold is incremented by 5 during region growing, more pixels surrounding the seed point within the trachea are identified. A stopping criterion is established to halt the region-growing process when the trachea has been adequately segmented.
In this technique lung segmentation and border tracking is done in two different sections, while they can be done in one step. Areas with high intensity might be abnormal regions in lung and histogram thresholding might lose these parts.

2.2 Texture Segmentation

Texture analysis and segmentation in discriminating between healthy and unhealthy lung tissue is an essential part of most Computer-Aided Diagnosis systems.
Texture analysis approaches are usually classified into four categories:

- structural
- statistical
- model-based
- transform methods

Structural approaches [18], [7] represent texture by well defined primitives (micro-texture) and a hierarchy of spatial arrangements (macro-texture) of those primitives. To describe the texture, one must define the primitives and the placement rules. The choice of a primitive (from a set of primitives) and the probability of the chosen primitive to be placed at a particular location can be a function of location or the primitives near the location. The advantage of the structural approach is that it provides a good symbolic description of the image; however, this feature is more useful for synthesis than analysis tasks. The abstract descriptions can be ill defined for natural textures because of the variability of both micro- and macrostructure. There is also no clear distinction between them. A powerful tool for structural texture analysis is provided by mathematical morphology [19], [20]. It may prove to be useful for bone image analysis, e.g. for detection of changes in bone microstructure.
Statistical approaches represent the texture indirectly by the non-deterministic properties that govern the distributions and relationships between the grey levels of an image. Methods based on second-order statistics (i.e. statistics given by pairs of pixels) have been shown to achieve higher discrimination rates than the power spectrum (transform-based) and structural methods [21]. Human texture discrimination in terms of texture statistical properties is investigated in [22]. Accordingly, the textures in grey-level images are discriminated spontaneously only if they differ in second-order moments. Equal second-order moments, but

different third-order moments require deliberate cognitive effort. This may be an indication that also for automatic processing, statistics up to the second order may be most important [23]. The most popular second-order statistical features for texture analysis are derived from the so-called co-occurrence matrix [18]. They were demonstrated to feature a potential for effective texture discrimination in biomedical-images [24]. The approach based on multi-dimensional co-occurrence matrices was recently shown to outperform wavelet packets (a transform-based technique) when applied to texture classification [25].

Model based texture analysis [26], [27], [28], [29], [30], which uses fractal and stochastic models, attempts to interpret an image texture by use of, respectively, generative image model and stochastic model. The parameters of the model are estimated and then used for image analysis. In practice, the computational complexity arising in the estimation of stochastic model parameters is the primary problem. The fractal model has been shown to be useful for modeling some natural textures. It can be used also for texture analysis and discrimination [27], [31], [32]; however, it lacks orientation selectivity and is not suitable for describing local image structures.

Transform methods of texture analysis, such as Fourier [33], Gabor [34], [35] and wavelet transforms [36], [37], [38] represent an image in a space whose co-ordinate system has an interpretation that is closely related to the characteristics of a texture (such as frequency or size). Methods based on Fourier transform perform poorly in practice, due to its lack of spatial localization. Gabor filters provide means for better spatial localization; however, their usefulness is limited in practice because there is usually no single filter resolution at which one can localize a spatial structure in natural textures. Compared with the Gabor transform, the wavelet transforms feature several advantages: first, varying the spatial resolution allows it to represent textures at the most suitable scale. Second, there is a wide range of choices for the wavelet function, so one is able to choose wavelets best suited for texture analysis in a specific application. These advantages make the wavelet transform attractive for texture segmentation. The problem with wavelet transform is that it is not translation-invariant

[39].

2.2.1 Previous Works

Lung parenchyma evaluation is done by several research group exclusively. Various texture segmentation methods, which are addressed in previous section, are utilized. In this section the existing texture segmentation methods which are exclusively utilized to evaluate lung parenchyma is discussed.

ANN Technique

In order to detect interstitial lung diseases, Uchiyama *et al.* [40] [41] developed a CAD scheme, in which lung regions are divided into many contiguous regions of interest with a 32 by 32 matrix. Six physical measures are determined for each region and artificial neural networks (ANNs) are employed to distinguish between seven different patterns including normal and abnormal lung tissue.

Later the number of features increased by the same group. 10 clinical parameters and 23 HRCT features have been utilized to differentiate among 11 diffuse lung diseases [42].

In this technique 32x32 matrices is used to evaluate the features. Lung occupies at most one third of the image size, which is 512x512. Choosing the size of 32 can be a cause of loosing some abnormalities in lung, particularly small abnormal regions. Uchiyama *et al.* claimed the sensitivity of 100% for honeycombing with the specificity of 88.1% for their technique, while the proposed technique in this thesis proves to be superior.

AMFM Technique

Uppaluri *et al.* developed an adaptive multiple feature method (AMFM) which uses 22 statistical measures to classify six tissue patterns [43], [44], [45]. Edgementation is utilized in AMFM to segment different textures of lung region [46]. Edgementation is a kind of split and merge method, the split part is accomplished by edge detection and merge is done based on statistical measures.

Uppaluri *et al.* use edgementation which splits the lung based on all existing edges and

then merge them based on similariites in statistical measures. Since lung region contains an abundance of edges (vessels, air tree, air sacs, artery branches etc.), this method is time consuming for this application. Uppaluri *et al.* [43] claimed that their work is especially successful for the detection of normal, emphysemalike, ground glass, and bronchovascular patterns of the lung parenchyma, while it is less successful for the evaluation of the honeycombing and the nodular patterns.

Chapter 3

Methodology

In the first part of this research a new approach based on both similarity and discontinuity properties of the image using fixed thresholding and Watershed transform is proposed to segment lung regions in the chest CT images. The second part is dedicated to segmentation of different textures of lung parenchyma by two approaches: entropy filtering and decomposing the lung regions into sub-images with different resolutions using wavelet transform. The focus of this research is on a particular texture named honeycomb texture. The employed techniques are described in detail.

3.1 Lung Segmentation

In this section a novel lung segmentation technique based on watershed transform is presented. Lung region is precisely marked with internal and external markers. The markers are combined with the gradient image of the original data and watershed transform is applied on the combined data to find lung borders. "Rolling ball" filter is used to smooth the contour and fill the cavities while preserving the original borders. The details of this technique are discussed in the following sections.

3.1.1 Watershed Transform

Watershed transform can be classified as a region-based segmentation approach. Buecher and Lantuejoul [47] formalized the concept and later Vincent and Soille [48] turned it into

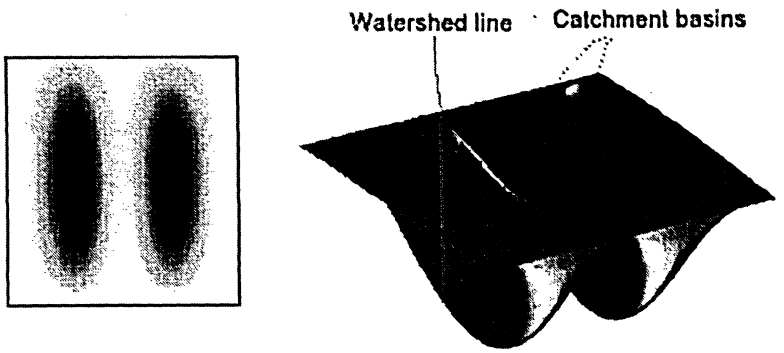

Figure 3.1: Watershed Lines and Catchment Basins (Courtesy of Steve Eddins).

an "immersion-based" algorithm. "Watershed" refers to a ridge that divides areas drained by different river systems. A "catchment basin" is the geographical area draining into a river or reservoir. Watershed transform finds "catchment basins" and "watershed ridge lines" in an image by treating it as a surface, where bright pixels are high and dark pixels are low [5]. Figure 3.1 illustrates the concepts of watershed lines and catchment basins.

Several definitions of the watershed transform have been declared. Marker-based watershed algorithms on discrete images [5], [49] are considered in this thesis. Generally, the watershed transform is computed on the gradient image, where the boundaries of the catchment basins are located at high gradient points. The principle of the immersion-based watershed algorithm [48] can be illustrated by imagining the gradient image as a relief (the elevations or inequalities of a land surface), with the height variable being the grey-value for each pixel position. Imagine, water immersing from the bottom of the relief (the darkest parts of image), every time the water reaches a minimum, which corresponds to a region in the original image, a catchment basin is grown. Watershed transform is based on set theory and can be formulated as follows:

$$T[n] = \{(x,y)|g(x,y) < n\} \tag{3.1}$$

In which, $g(x,y)$ denotes the gradient image of the original one. n is the level of water and $T[n]$ represent the set of coordinates (x,y) for which $g(x,y)$ is less than n. In other

words $T[n]$ is the set of coordinates of points in $g(x,y)$ lying bellow the plane $g(x,y) = n$. Assume $M_1, M_2, ...$ are the sets of pixel coordinations in the regional minima of an image $g(x,y)$. A portion of binary image $T[n]$ at the stage n of flooding that is associated with regional minimum M_i is given by:.

$$C_n(M_i) = C(M_i) \bigcap T[n] \tag{3.2}$$

$C_n(M_i)$ is the set of pixel coordinations in the catchment basin associated with minimum M_i that are flooded at stage n. $C(M_i)$ is a set of pixel coordinations in the catchment basin associated with regional minimum M_i.
Finally $C[n]$, which denotes the union of R flooded catchment basins portions at stage n, is formulated as:

$$C(n) = \bigcup_{i=1}^{R} C_n(M_i) \tag{3.3}$$

$C[n]$ can be considered as regions of interest.

When two neighboring catchment basins eventually meet, a dam is created to avoid the water merging at that level of flooding and spilling from one basin into the other. This property is utilized to make the left and right lung separation during the transformation. As it is shown in figure 3.2, when the water reaches the maximum gray-value, the union of all dams forms the watershed lines [5].

Watershed transform has several advantages: it is a simple intuitive method, which is fast and can be parallelelized [50], [51].
Over-segmentation is a well-known drawback in watershed segmentation. Since every regional minimum, even if tiny and insignificant, forms its own catchment basin, over-segmentation occurs. This phenomenon is illustrated in figure 3.3-c, which is the result of applying standard watershed transform on the gradient image of a pulmonary CT slice (figure 3.3-a). By using marker-based watershed transform, we can decrease the regional minima and bind

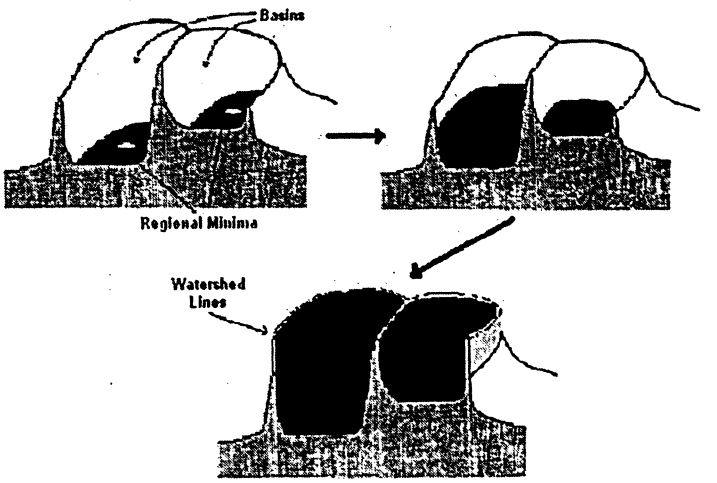

Figure 3.2: The process of building Watershed Lines (Courtesy of Tesi di Laurea).

them within the region of interest to prevent over-segmentation. There are several techniques to define markers and choosing a technique is highly dependent on the application. The details of our approach are described in the following steps.

3.1.2 Gradient Image (Step 1)

Since watershed transform is applied on the gradient image, the first step is to obtain the gradient image. The Sobel masking operator is applied on the original pulmonary CT image in both horizontal and vertical directions to create the gradient image (figure 3.3-b).

3.1.3 Internal Marker (Step 2)

The key point of our approach is the internal markers. The internal markers are the connected components of the pixels with almost the same intensity values, whose external boundary pixel values are all greater than a level of n. The value of n is a gray level value, which specifies the approximate gray level value for non-body pixels in CT images. In pulmonary CT images the air will appear with the intensity of -1000 Hounsfield Units (HU) (refer to

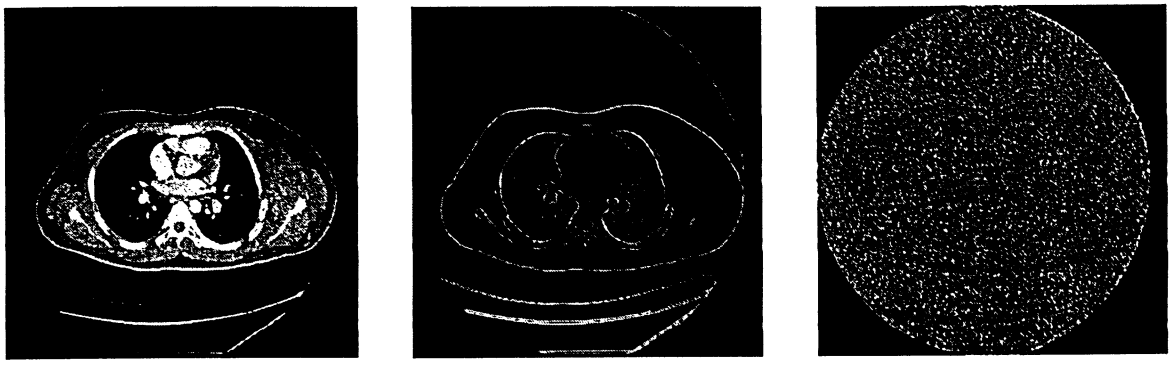

(a) (b) (c)

Figure 3.3: (a) Original pulmonary CT image. (b) The gradient image of figure (a) using Sobel masking. (c) Result with oversegmentation obtained using standard watershed transform on the gradient image.

Appendix B.1.1). Since lung region is filled with air sacs, blood vessels, capillaries and air tree, it will be in the range of -1000 to -400 HU. The chest wall, blood and bone will be much dense and well above -400 HU. In order to specify the internal markers the regions with pixel values lower than -400 HU are selected. The background of the CT image is almost black (lower than -400), so, it makes an erroneous regional minimum. Background is removed by eliminating the objects, which are attached to the border of the binary image [52]. After removing the background, the small objects in the markers, which are caused by the cross-section of veins, should be eliminated. The open morphological operator is utilized to eliminate these small separate objects. The result is shown in figure 3.4-a. To remove trachea and other large airways from the internal marker binary image, two methods are utilized and compared with each other. The first method is simply to remove the small isolated objects near the center of the chest in the CT image, which is accurate and fast. The second method is based on Masutani's work [13]. The location of the trachea is identified by searching for the circular object near the center of first few slices. Each slice provides the seed point for the next slice. When the size of the region on a slice highly increases, the region growing procedure stops and the pixels, which correspond to trachea or main bronchi, are turned off in the internal marker binary image. In this method elimination of trachea in

each slice is depending on the previous slice, while in the first method it is done in each slice independently.

In CT images with certain disease conditions such as emphysema, the left and right lungs are attached to each other or separated with a very thin wall (with the intensity lower than -400 HU). A single large lung region in the internal marker binary image indicates that the left and right lung regions are merged. To extract the border in this case along with other tissues during the watershed transform, no regional minimum should be imposed on the area between the two lung regions. This area is specified by a black strip near the center of the chest in the image. The pixels of the internal marker on this area are turned off to avoid imposing regional minima on this area.

3.1.4 External Marker (Step 3)

Lung border is located in the neighborhood area of the internal marker. To bind this area an external marker is required. The internal marker is dilated with two circular structuring elements with the ratios of 4 and 104. By subtracting the results, external marker is specified. It is a wide strip around the internal marker with a small distance. The width of the strip is selected at least 100 pixels to eliminate the whole possible minima in the neighborhood. The distance between the two markers is 3 pixels to include the slightly curved border of the lung. The wider the strip, the lower the risk of oversegmentation. The ratio of the smaller structuring element specifies the distance between the two markers. Figure 3.4-b shows the external marker for the lung CT image of figure 3.3-a.

3.1.5 Imposing Regional Minima (Step 4)

In this step the regional minima will be placed only in the marked area of the gradient image. To do this, it is required to compute the watershed lines in the region of interest. Minima imposition procedure, which utilizes morphological reconstruction, is used to place regional minima only within the area of the union of the two markers (figure 3.5-a).

(a) (b)

Figure 3.4: (a) Internal Marker (b) External Marker.

(a) (b)

Figure 3.5: (a) Imposed regional minima in the marked area. (b) Segmented lung contour.

3.1.6 Watershed Transform (Step 5)

Watershed transform of the obtained image finds the watershed lines corresponding to the most significant edges between the markers. These watershed lines are the borders of the lung regions (figure 3.5-b). Since during this transform a dam is created between the two lung regions to prevent merging, the thin wall between the attached left and right lung with emphysema disease is also extracted.

(a) (b)

Figure 3.6: (a) Smoothed lung contour using rolling ball filter (b) Segmented lung regions.

3.1.7 Smoothing and Filling the Cavities (Step 6)

This is one of the most common practices in many lung segmentation schemes [10], [52]. In some CT images, the segmented lung region excludes dense structures, such as juxtapleural nodules and hilar vessels (figure 3.5-b). To include these structures the rolling ball filter is utilized [5], [52]. The segmented lung border is superimposed on the original image and the closed morphological operator is applied. A rolling ball with the ratio of 9 is selected as a 3D structuring element. Indeed, the ball rolls along the lung contours identifying the pixel along the balls circumference with tangential slope that matches the tangential slope of the lung contour at the current contour pixel. The width of entering blood vessels in children is about 1cm. The indentation of the vessels are fairly smoothed by a ball with the ratio of 9. The smoothed image is shown in figure 3.6-a. At this stage those parts of the border that need to be smoothed are changed and other parts remain the same, which is the unique advantage of our technique. The segmented lung regions are shown in figure 3.6-b.

3.2 Honeycomb Lung Segmentation using Entropy Filtering

Several interstitial lung diseases could be diagnosed based on Honeycombing feature. Figure 3.7 shows two CT images of honeycomb lungs.

Figure 3.7: Two lung CT images with honeycombing [2].

3.2.1 Spectral Measures

Spectral measures are suited for describing the periodic or almost periodic 2-D patterns. These measures are based on the Fourier spectrum and the patterns can be detected as concentrations of high-energy bursts in the spectrum. By expressing the spectrum in polar coordinates $S(r, \theta)$, the interpretation of spectrum features will be more meaningful. Analyzing $S_\theta(r)$ for a fixed value of θ yields the behavior of the spectrum (such as the presence of peaks) along a radial direction from the origin, and analyzing $S(\theta)$ for a fixed value of r yields the behavior along a circle centered on the origin. To obtain the global description of the spectrum the integrations of these functions are used:

$$S(r) = \sum_{\theta=0}^{\pi} S_\theta(r) \tag{3.4}$$

$$S(\theta) = \sum_{r=0}^{R_0} S_r(\theta) \tag{3.5}$$

where R_0 is the radius of a circle centered at the origin. Three 50 by 50 images are selected from the different parts of the lung CT images (figure 3.8) and the equations B.1 and 3.13 are computed for each. The selected images show healthy, honeycomb and the part with vessel branches of lung tissue. The results of above equations are shown in figures 3.9 and 3.10.

As it is shown, there are a few differences between the results for different types of the lung tissue, so, the required information to detect the honeycomb tissue cannot be obtain

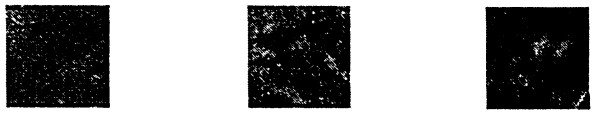

Figure 3.8: Healthy, Honeycomb and tissue with vessel branches.

using these equations. These measures are usually useful for distinguishing periodic from non-periodic patterns. For periodic patterns S_θ is symmetrical and can be distinguishes from non-periodic patterns.

3.2.2 Statistical Measures

Statistical measures of intensity histogram are frequently used to analyze textures. Some of these measures are based on statistical moments. The *nth* moment about the mean is given by:

$$\mu_n = \sum_{i=0}^{L-1}(z_i - m)^n p(z_i) \tag{3.6}$$

where z_i is a random variable indicating intensity, $p(z_i)$ is the histogram of the intensity levels in a region, L is the number of possible intensity levels, and m in equation 3.7

$$m = \sum_{i=0}^{L-1} z_i p(z_i) \tag{3.7}$$

is the mean intensity. Another statistical property which is commonly used for texture analysis is "Standard Deviation", which is a measure of average contrast and is expressed by:

$$\sigma = \sqrt{\mu_2(z)} \tag{3.8}$$

Smoothness is another measure to discriminate different textures and is defined by:

$$R = 1 - 1/(1+\sigma^2) \tag{3.9}$$

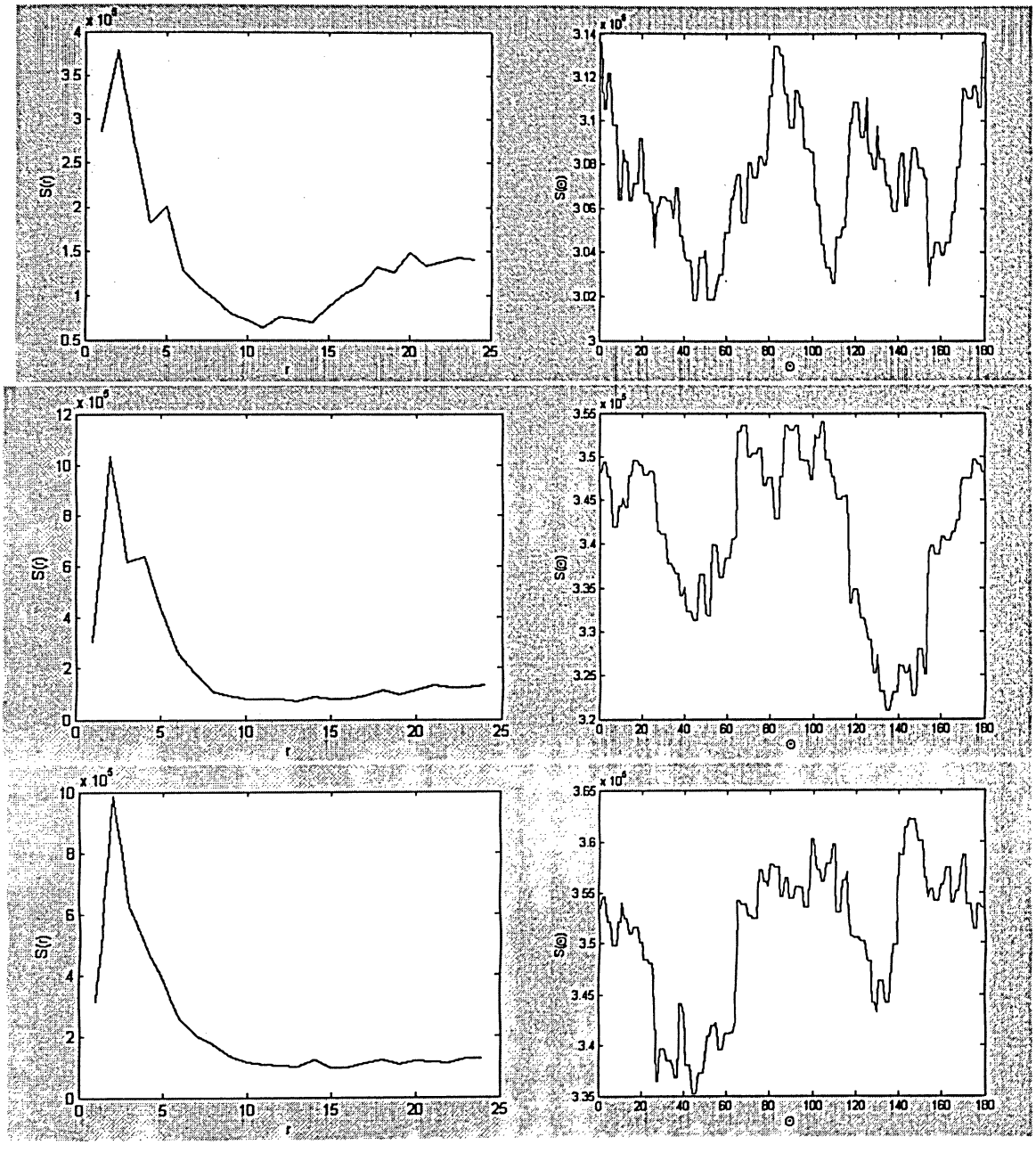

Figure 3.9: : Left: S(r) Right: $S(\theta)$ of healthy, honeycomb and area with vessel branches.

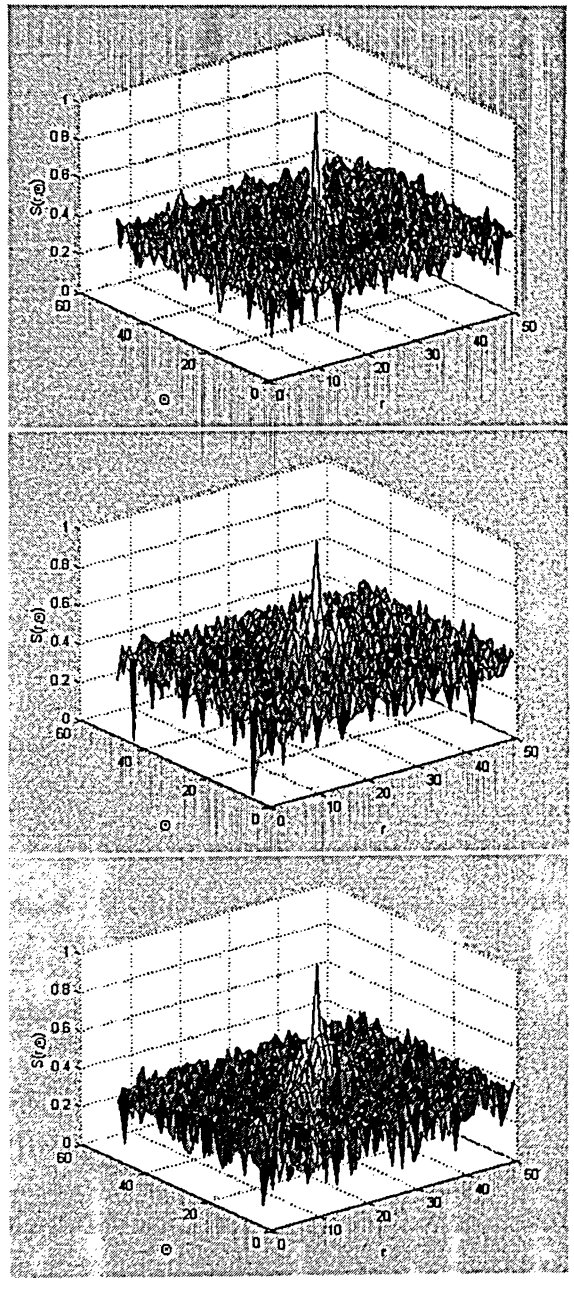

Figure 3.10: $S(r, \theta)$ of healthy, honeycomb and nodular.

Table 3.1: Statistical Measures of Three Lung Different Tissue

	scale	Healthy	Honeycomb	Vessel Branches
Mean	1.0e+004	1.1505	1.2248	1.2702
Third Moment	1.0e+003	1.7085	2.4324	2.3208
Smoothness	1	0.4469	0.9017	0.8215
NTM	1	-3.3794	-6.3223	2.8445
Uniformity	1	18.2679	16.3927	21.8349
Entropy	1	276.8342	341.2825	303.6690

Uniformity is maximum when all gray levels are equal and expressed by:

$$U = \sum_{i=0}^{L-1} p^2(z_i) \tag{3.10}$$

Entropy is a measure of randomness and is defined as:

$$e = -\sum_{i=0}^{L-1} p(z_i) \log_2 p(z_i) \tag{3.11}$$

All these six features are tested for three different types of lung parenchyma and the result is tabulated in table 3.1. The measures are scaled by 100. One of the reliable measures for the purpose of this paper is Entropy, which is used to segment the honeycomb region and is discussed in detail in the next part.

3.2.3 Entropy Filter

As a part of this research entropy is utilized to segment honeycomb region of lung tissue. The concept of entropy in information theory describes how much randomness (or, alternatively, 'uncertainty') there is in a signal or random event. An alternative way to look at this is to talk about how much information is carried by the signal. In an image, regions with more variations in intensity have higher entropy. In order to detect the areas with higher

resolutions of an image, it is filtered by an entropy filter, which replaces each pixel value with the entropy value of itself and its 9 by 9 neighborhood pixel values. Figure 3.12 shows the result of entropy filtering of the lung CT image in figure 3.11.

Figure 3.11: CT image of Honeycomb Lung.

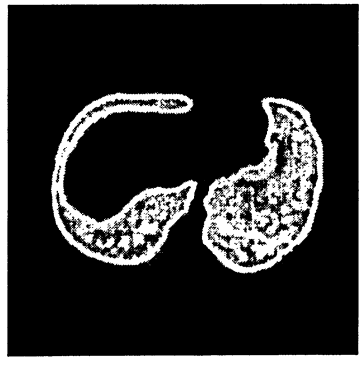

Figure 3.12: Entropy filtered image.

The area with honeycombing and vessel branches has high intensity variation and higher entropy value therefore they look brighter in the entropy filtered image. The next step is to threshold the filtered image to extract the area with higher entropy. To accomplish this task a fixed threshold with the value of 230 has been used. The binary image after thresholding is shown in figure 3.13. Since regions with vessel branches and the borders of the lung have also high entropy, these regions are also extracted along with the honeycomb lung.

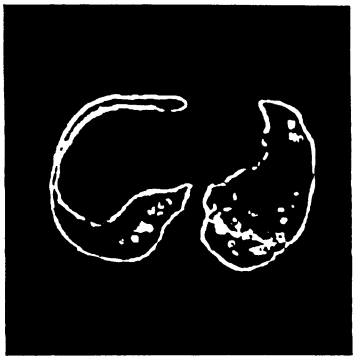

Figure 3.13: Thresholded filtered image.

3.2.4 Extracting Honeycomb from other Textures

Honeycombing is a set of cysts filled with air, whereas the vessel branches and the lung border are denser than the air. In other words in CT image honeycombing is seen as dark holes but lung border and nodular parts are seen as brighter areas. This feature is used to distinguish honeycomb pattern from others. The binary thresholded image is used as a mask on the original image to keep the darkest areas of the thresholded image (figures 3.15 and 3.15).

Figure 3.14: Original gray scale pixel values of thresholded image.

2D seeded-region growing is used to extract the regions with honeycomb tissue. The first step is to find seeds. Dilation morphological operation is utilized to eliminate small isolated

Figure 3.15: Darkest areas of the thresholded image.

objects (figure 3.16). The next step is to build a mask. The darkest regions of high resolution

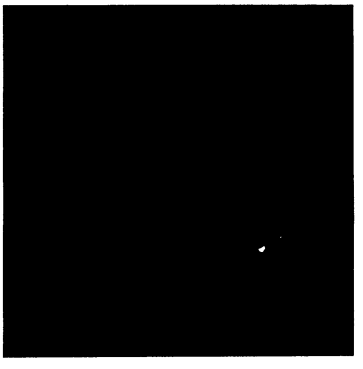

Figure 3.16: Seeds.

areas, which are obtained previously (figure 3.15), are dilated by a disk-structuring element with the ratio of 3 to include the honeycomb hole walls and have almost the natural size of the abnormal region (figure 3.17). The disk structuring element has been chosen because of the circular shape of the honeycomb holes.

The final step is to apply 2D region growing technique on the obtained mask and seeds, which are shown in figures 3.16 and 3.17. 8-connected neighborhoods and the fast hybrid grayscale reconstruction algorithm described in [53] is utilized to perform region growing. The result is a binary image (3.18) which is used as a mask to extract honeycomb area from

Figure 3.17: The mask used for region growing.

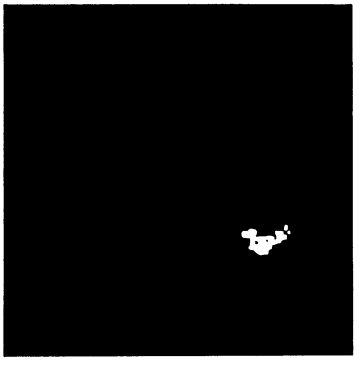

Figure 3.18: The mask for honeycomb area.

the original image. Figure 3.19 shows the abnormal lung tissue and illuminates the accuracy of this method.

3.3 Honeycomb Lung Segmentation using Wavelet Transform

This section is dedicated to the second proposed approach of honeycomb lung segmentation by decomposing the image of lung region into separated images with different resolution using wavelet transform.

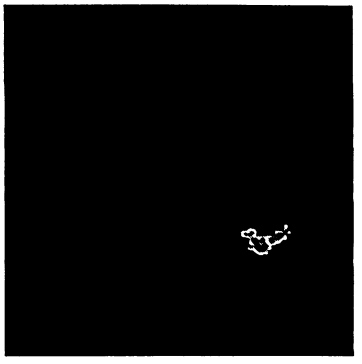

Figure 3.19: Extracted honeycomb tissue of the lung.

3.3.1 Wavelet Transform

Recently, multiresloution-based approaches have drawn increasing attention in the field of texture analysis. Several successful applications of this approach to automatic texture segmentation have been proposed. Wavelet transform [36] is used in multiresolution-based approaches. Most of the wavelet-based methods use a pyramidal type of decomposition to transform the input image into an image of wavelet coefficients at different resolutions. The wavelet coefficients are then transformed into texture-specific features. Based on the features, traditional clustering techniques such as c-means are adopted to segment the image into texture regions.

Wavelet analysis is the breaking up of a signal into shifted and scaled versions of the original (or mother) wavelet. General formula for continuous wavelet transform can be written as:

$$\Psi_{s,\tau}(t) = \frac{1}{\sqrt{s}}\Psi\left(\frac{t-\tau}{s}\right) \tag{3.12}$$

$$\gamma(s,\tau) = \int f(t)\ \Psi^*_{s,\tau}(t)\ dt \tag{3.13}$$

Where Ψ is a wavelet, which is a waveform of effectively limited duration that has an average value of zero. The signal f(t) is filtered by the shifted and scaled versions of this filter to decompose it into different frequency bands. The values of γ for different scales (s) and translations (τ) are the coefficients of transformed signal.

In the proposed approach discrete wavelet transform is utilized. The discrete wavelet transform of image f(x,y) of size M by N can be written as [5]:

$$W_{\Phi}(j_0, m, n) = \frac{1}{\sqrt{MN}} \sum_{x=0}^{M-1} \sum_{y=0}^{N-1} f(x,y) \Phi_{j_0,m,n}(x,y) \tag{3.14}$$

$$W_{\Psi}^{i}(j, m, n) = \frac{1}{\sqrt{MN}} \sum_{x=0}^{M-1} \sum_{y=0}^{N-1} f(x,y)\ \Psi_{j,m,n}^{i}(x,y) \tag{3.15}$$

$$i = \{H, V, D\}$$

$\Phi_{j_0,m,n}(x,y)$ and $\Psi_{j,m,n}^{i}(x,y)$ are the scaled and translated basis functions:

$$\Phi_{j,m,n}(x,y) = 2^{\frac{1}{2}} \Phi(2^j x - m, 2^j y - n) \tag{3.16}$$

$$\Psi_{j,m,n}^{i}(x,y) = 2^{\frac{1}{2}} \Psi^{i}(2^j x - m, 2^j y - n) \tag{3.17}$$

$$i = \{H, V, D\}$$

$\Phi(x,y)$ is the scaling function and $\Psi^{H}(x,y)$, $\Psi^{V}(x,y)$, and $\Psi^{D}(x,y)$ are three two-dimensional wavelets, which are the products of one-dimensional Φ and corresponding wavelet Ψ. i is a superscript that identifies the directional wavelets [5].

Discrete wavelet transform corresponds to multiresolution approximation expressions. Multiresolution analysis is carried out using 2 channel filter banks composed of a low-pass and a high-pass filter and each filter bank is then sampled at a half rate (1/2 down sampling) of the previous frequency. By repeating this procedure, it is possible to obtain wavelet transform of any order. Filtering is implemented in a separable way by filtering the lines and columns so the original image can be transformed into approximation, horizontal, vertical and diagonal sub-images.

Among several well known wavelets including Haar, Daubechi1, Daubechi2 and ..., which have been tested, BiorSplines 1.1 wavelet proved to have best results for this application. The horizontal, vertical and diagonal subimages obtained from applying wavelet transform on lung image using BiorSplines 1.1 wavelet are shown in figure 3.20 after upsampling. Since honeycomb region is best differentiable in horizontal and vertical subimages, they are good candidates to extract honeycomb regions.

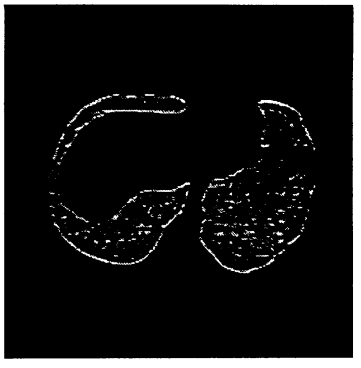

(a) Horizontal subimage

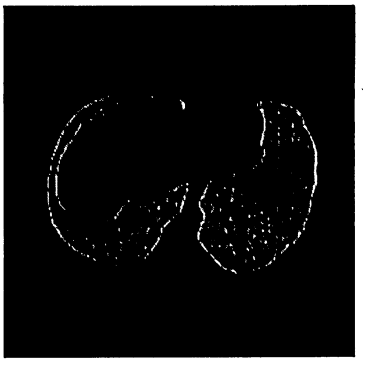

(b) Vertical subimage

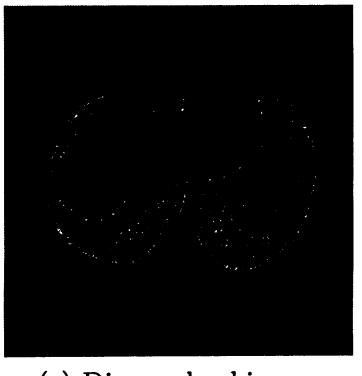

(c) Diagonal subimage

Figure 3.20: Wavelet Transform.

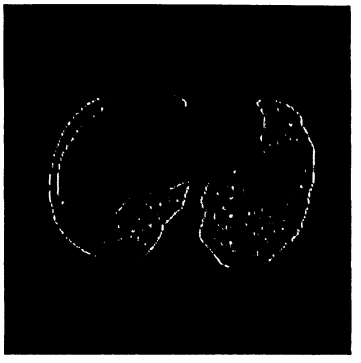

Figure 3.21: High resolution regions.

Figure 3.22: Masking high resolutions areas on original image.

3.3.2 Histogram Thresholding

To keep the high resolution areas histogram thresholding [5] is used. The vertical subimage (figure 3.20) is used to extract the high resolution areas. The binary image of the lung area is used as a mask to calculate the histogram of vertical subimage of the lung region. The result of thresholding is shown in figure 3.21.

3.3.3 Extracting Honeycomb from other Textures

Honeycombing is a set of cysts filled with air, where as areas with artery branches and lung border are denser than the air. In other words in a lung CT image honeycombing is seen as dark holes but lung border and artery branches are seen as brighter area. This feature is used to distinguish honeycomb pattern from other high resolution areas. To extract the

low intensity regions with high resolution the thresholded images is used as a mask on the original image 3.22. To find darkest areas of the thresholded image, the regions with pixel values less than -800 Hounsfield Unit (around the gray level value of air) are kept.
Seeded-region growing is used to extract the exact parts of honeycomb tissue. To find accurate seeds and eliminate small regions from low intensity regions with high resolution, morphological erosion with a vertical line structuring element with the length of 5 is used (figure 3.23-a). The length of 5 experimentally proved to be the proper length to keep the seeds. To have an accurate mask for region growing method the darkest high resolution objects are dilated by a disk structuring element of size 5 (figure 3.23-b). Since honeycomb region has circular holes a disk structuring-element is selected. The final step is to apply region growing technique with the seed shown in figure 3.23-a on the mask shown in figure 3.23-b. The result is shown in figure 3.24 which shows the accuracy of this method.

(a) (b)

Figure 3.23: a) Seed or marker, b) Mask.

A Graphical User Interface has been also developed to test the proposed techniques (figure 3.26).

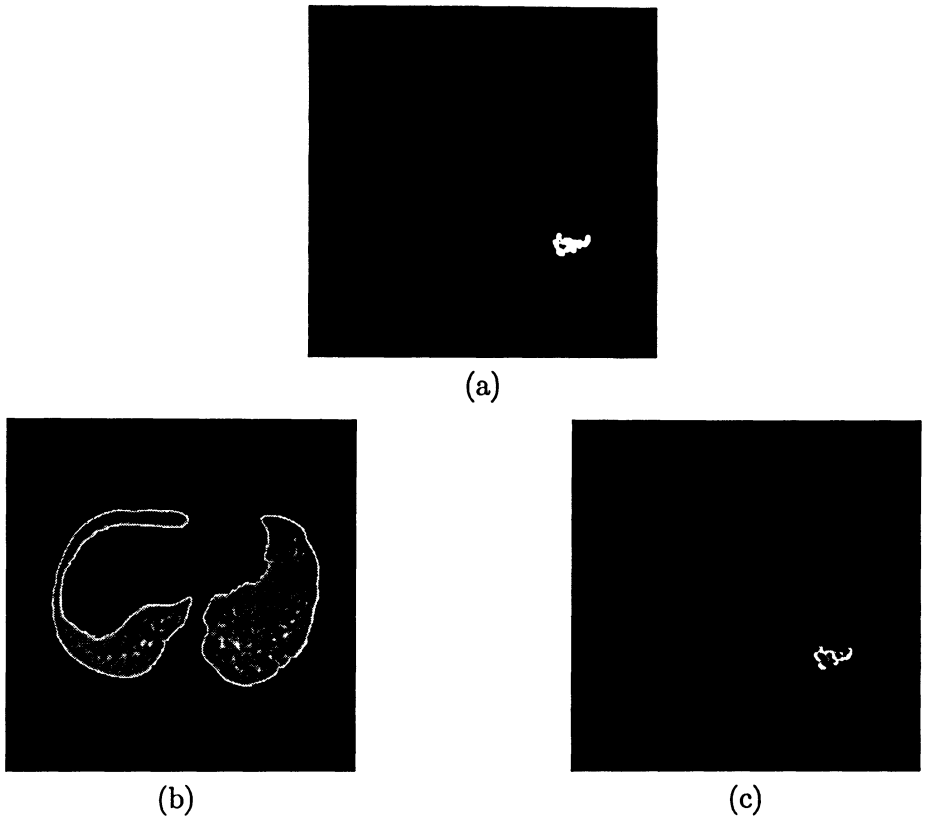

Figure 3.24: a) Result of region growing, b) Lung with honeycombing, c) Segmented honeycomb area.

Figure 3.25: a) Original slice with honeycoming, b) Segmented honeycomb area.

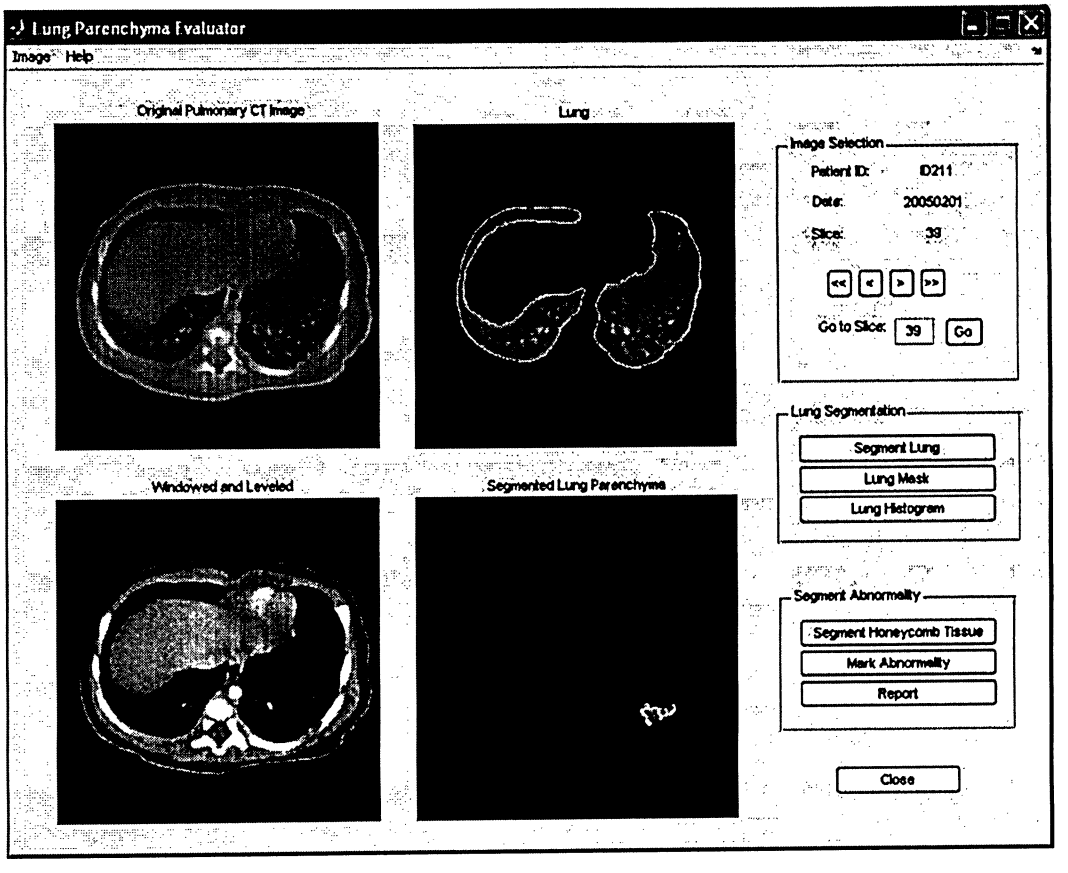

Figure 3.26: Graphical User Interface which is developed to test the proposed algorithms.

Chapter 4

Validation

This chapter is dedicated to demonstrate the feasibility and usefulness of the proposed approaches. The evidences for each technique is discussed in separate sections.

In the first section lung segmentation method is evaluated using experimental results. The proposed technique has been applied on several pulmonary CT images and the segmented lung regions have been assessed by a radiologist. It is also compared with a technique proposed by a group of researchers in University of Iowa [10]. The comparison is made based on accuracy and speed.

In the second section the detection of abnormal lung tissue is assessed to validate the proposed composite technique. Statistical analysis is done as an evaluation technique.

The tests have been applied on 512 by 512 by 16 pediatric Helical CT images. The images are acquired by a GE MEDICAL SYSTEMS CT scanner from the Department of Diagnostic Imaging in the Toronto Hospital for Sick Children. All approaches are implemented in MATLAB 7.0.

4.1 Lung Segmentation Verification

The test procedure of lung segmentation method has been accomplished in two stages. This method is applied on more than 180 CT and the segmented lung regions have been visually verified. Some examples are given in the next part of this section. In the second part of this section the proposed technique is compared with a commonly used method [10] based on speed and accuracy.

4.1.1 Experimental Results

The pictorial lung segmentation results for 512 by 512 by 16 3D helical CT images of thorax with different slice thicknesses are given. The slices are selected from different parts of the chest to show the accuracy of the proposed technique. The results for the images of upper, middle and lower parts of the chest with various regions of the lung, which are successfully segmented, are shown in figure 4.1.

To make the borders smooth and retrieve the dense structures, which are adjunct to the lung border (figure 4.2-a), a "rolling ball" with the ratio of 9 is used. The images in figures 4.2-b and 4.2-c illustrate the segmented lung borders before and after the rolling ball filtering. Comparing the segmented lung regions (figure 4.2-d) with the original image (figure 4.2-a) verifies the accuracy of this technique.

The theory of Watershed transform along with the experimental results prove that even if there are no strong edges between the internal and external markers, watershed transform always detects a significant edge in the desired area that demonstrates the robustness of this technique. This method has been applied on more than 180 CT images from different parts of the chest and the results are visually acceptable.

4.1.2 A Comparison

In this part of testing procedure a comparison is made between the proposed method and Hu's work. As addressed in chapter 2, Hu *et al.* [10] proposed a method for lung segmentation based on optimal thresholding. As a part of this research Hu's work is developed and

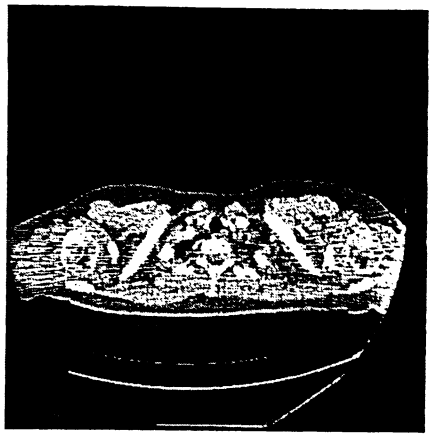

(a)Upper part of chest.

(b)Upper part of lung.

(c)Middle part of chest.

(d)Middle part of lung.

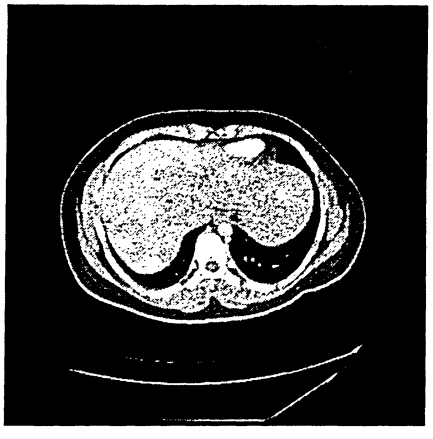

(e)Lower part of chest.

(f)Lower part of lung.

Figure 4.1: Left: Original CT images. Right: Segmented lung Regions.

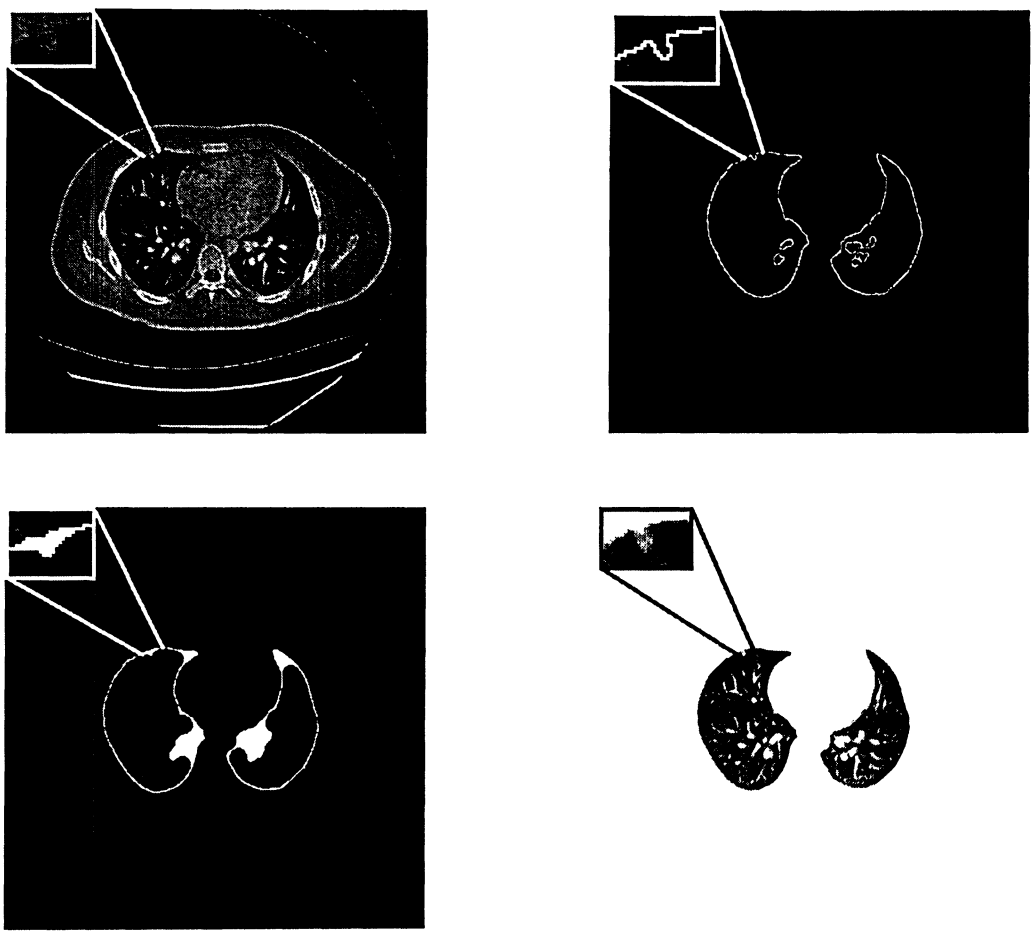

Figure 4.2: (a) Originl pulmonary CT image. (b) Segmented lung borders. (c) Smoothed lung borders. (d) Lung regions.

compared with the proposed technique. The popularity of Hu's method provides a good incentive to be chosen for comparison purpose.
A dataset of a patient with a high stage of honeycomb lung is selected. Both methods are applied on the dataset. As it is shown in figure 4.3 the Hu's method is less successful identifying left lung area, whereas the proposed is fairly successful.

In terms of speed the two methods were tested on the same computer with the same dataset. For each slice with our method it takes less than 5 seconds to do the segmentation task including reading image files, ordering them, segmentation and smoothing the borders , whereas Hu's method takes about 7 seconds.
Both tests illuminates the superiority of our method based on speed and accuracy.

4.2 Abnormal Lung Tissue Segmentation

The images, which were used to test the proposed technique are 512x512x16, 3D helical CT with the slice thickness of 1.25 millimeter. This method has been tested on 91 pediatric chest CT images containing healthy and unhealthy lung (with honeycomb patterns) images and the results revealed the accuracy and the speed of the proposed composite method. The specifications of the test datasets is tabulated in table 4.1. It has been tested on a Pentium IV 2.8 GHz PC with 512 MB RAM and the average required time for each slice was 4-5 seconds. Since the area of lung region varies in different slices, the execution time varies for each slice.

One approach used to define the accuracy of an imaging system is to evaluate the systems sensitivity and specificity. Sensitivity, also called true positive fraction (TPF), is the probability of diagnosing the presence of disease when it is actually present. Specificity, also called true negative fraction (TNF) is the probability of identifying the absence of disease when it is not present. This thesis addresses the use of Statistical analysis to evaluate the accuracy of the new composite method, as compared to other existing methods. The statistical analysis is tabulated in table 4.2.

Table 4.1: Datasets Specifications

Test Sets	Date of Acquisition	Images	Healthy Images	Images with Abnormality
TST-1	20050201	57	48	9
TST-2	20040803	10	1	9
TST-3	20041216	24	24	0

Table 4.2: Statistical Analysis of the Composite Method

Patient ID	Number of FPs	Number of TPs	FP (%)	Sensitivity (%)	Specificity (%)
TST-1	1	9	1.75	100	97.91
TST-2	0	9	0	100	100
TST-3	3	0	12.5	100	87.5

Although there is not any common database of lung CT images with different diseases we can compare the sensitivity and specificity of our approach with the two existing approaches, which are addressed in chapter 2.

Uppaluri *et al.* [43] evaluated their method by the kappa statistic of agreement between the regions, for which the majority of the observers agreed on a pattern type, versus the computer. The AMFM has demonstrated to be especially successful for the detection of normal, emphysemalike, ground glass, and bronchovascular patterns of the lung parenchyma (individual Kappa 0.6). Uppaluri *et al.* claimed that the AMFM with the sensitivity of 82.5% and specificity of 99.9% is less successful for the evaluation of the honeycombing and the nodular patterns (individual Kappa 0.2). For this sensitivity and specificity, Uppaluri *et al.* utilized a test set which includes their training set aswell.

Uchiyama *et al.*, who proposed an ANN method to detect different lung diseases, claimed the sensitivity of 100% for honeycombing with the specificity of 88.1% for 98 datasets. Since their method use the blocks of 32 by 32 to calculate the statistical features and segment the regions, it might lose small regions with abnormal texture.

In Both techniques the researchers use an abundance of statistical measures which makes

the process very slow.

Comparing our Composite method with Hu's and Uchiyama's techniques elucidates that the proposed technique is very promising.

The drawback of the technique is that although it detects all honeycomb areas, the boundary of the segmented abnormal area is not accurate. This issue opens an area for further research and improvement of the proposed method.

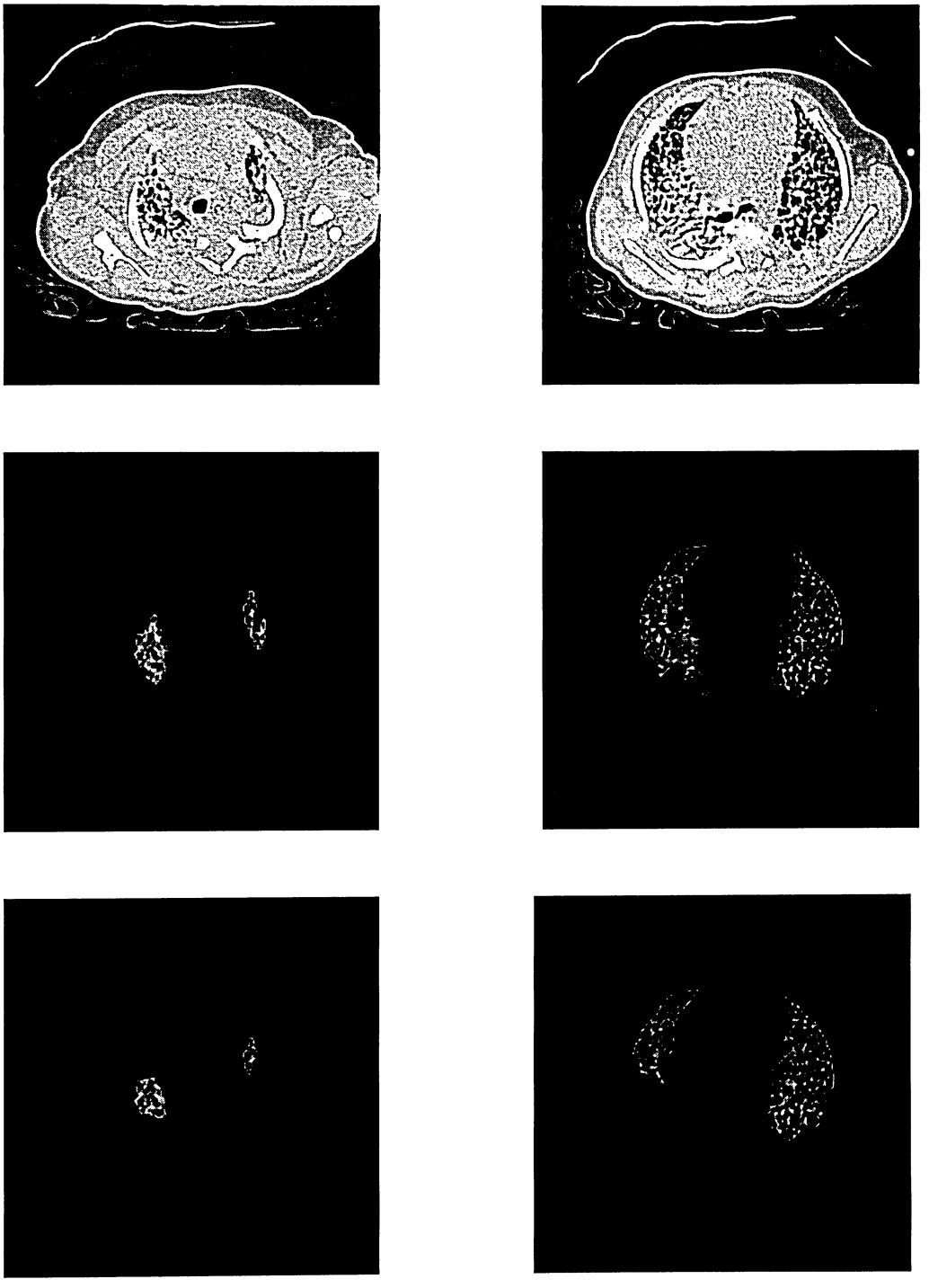

Figure 4.3: First row: Original Chest CT Image. Second Row: Segmented Lung with Watershed Transform. Third Row: Segmented Lung with Optimal Thresholding.

Chapter 5

Conclusions and Future Works

This chapter represents the conclusion of the thesis. It gives an overview of the research including a summary of accomplishments and contributions of this thesis. The chapter closes with a discussion of the limitations of this work and recommendations for future research directions.

Computed Tomography is one of the most commonly used techniques to diagnose and quantify different diseases. Since the volume of CT images and the number of the repetition of studies have been increased, computer-aided diagnosis (CAD) schemes have a tremendous impact on the interpretation of medical images. Although CAD systems have been improved vastly, it is still almost exclusively the work of humans (radiologists) to interpret medical images and CAD systems act as a second tool to detect the abnormalities. To diagnose pulmonary diseases, chest CT images are investigated and the corresponding CAD systems are being developed by several research groups all over the world.

Lung segmentation is the first step of most pulmonary CAD systems. Limiting further processes to the lung areas saves time and resources like memory and CPU usage. The two most important issues in lung segmentation is accuracy and time. Inaccurate segmentation can be the cause of losing abnormalities in lung especially around the borders. As addressed in Chapter 2, various lung segmentation approaches have been proposed by other research groups. Several image segmentation techniques have been utilized by these approaches. Some of the existing methods are not fully automated while others are not very accurate or

they use heuristic techniques, which are time consuming. The first goal of this thesis was to propose, develop and evaluate a novel lung segmentation technique, which is superior to existing methods based on accuracy and speed. Watershed transform is the core transform in the proposed technique. It is applied on marked gradient image to find the borders and then a "rolling ball" filter smooths the extracted borders. This method has been developed along with another existing method which is commonly used to segment lung regions.
To detect and quantify the abnormalities, patterns of lung tissue in CT images are investigated by radiologists. In CAD systems, this task is accomplished by texture segmentation and analysis. Several research groups are working on improving the existing methods.
The next goal of this research is to propose a new texture segmentation method to extract the abnormal areas of lung tissue. Two techniques are proposed and developed to detect honeycomb abnormality in CT images. In the first proposed method, entropy filtering, which is a local filtering, is utilized to find high entropy areas. Entropy filtering replaces each pixel value with the entropy of itself and its neighbor pixels. Then seed based region growing is applied to find abnormality. The second method is a new composite method, which is composed of a multi resolution technique and the methods based on intensity similarities. In this technique wavelet transform is utilized to extract the high resolution areas of lung tissue. Since normal tissue of lung is almost plain in CT images, the high resolution areas include abnormalities along with normal areas with several vessel branches. To exclude normal areas with vessel branches, intensity values are compared to keep only darker areas . Seed based region growing is applied to find the region of interest. The results from both techniques are compared.

5.1 Conclusion

A novel lung segmentation method is developed and tested on several datasets. Optimal thresholding technique is developed and compared to the proposed method. As it is addressed in chapter 4, the results shown the accuracy and the speed of the novel method. Even if there are no strong edges between the internal and external markers, watershed transform

always detects a significant edge in the desired area and this capability demonstrates the robustness of our technique. This technique is applied on more than 180 paediatric pulmonary CT images from the Toronto Hospital for Sick Children and the results are visually acceptable and are approved by a radiologist. The drawback of this method is over-segmentation. It usually happens on low quality CT images.

A new composite technique is proposed and developed to evaluate lung tissue. In this method wavelet transform is utilized combined with intensity similarities. The proposed technique is robust, accurate, and fast. As it is discussed in chapter 4, it has been tested on several datasets and compared with other methods based on speed, sensitivity and specificity. The result reveals the robustness of the proposed approach.

The drawback of this technique is that although it detects all honeycomb regions, the contours of the segmented abnormal area is not accurate. This issue is an area that needs further research and improvement.

5.2 Future Works

This research opens a wide area of future research. The proposed method for lung segmentation has a good potential to detect the borders of pulmonary nodules, which is a very active research area.

Instead of marker-based watershed transform, the combination of watershed transform and distance transform can be utilized to separate attached nodules to improve the values of sensitivity and specificity in assessment of nodule detection.

The proposed lung tissue evaluation approach can be further improved to detect all possible abnormalities with different types of textures in lung tissue. Different patterns have different resolutions and the proposed method has the capability of detecting other textures of lung tissue, for example by applying multilevel thresholding on the transformed image different abnormal patterns can be segmented.

Automatic lung disease quantification is another field of research which is done on segmented abnormal region in CT images. It can also be used to monitor the healing process of the

disease.

In addition, this approach can be improved to localize the abnormal area accurately. This can be used in three dimensional visualization of lung and providing an idea of the shape and volume of abnormal region.

Virtual bronchoscopy is another active research area. Lung texture analysis and segmentation can also be utilized in developing a virtual bronchoscope.

Appendix A

The Anatomy of Lung

Lungs are anatomically divided into the left and right lung based on their locations with respect to the chest wall and rib cage [1]. The left and right lungs have five distinct anatomic compartments called lobes. The physical boundaries between the lung lobes are called lobar fissures, which allow the lobes to slide relative to each other, thus to accommodating shape changes of the thoracic cavity. There are three lobes in the right lung: the right upper lobe (RUL), the right middle lobe (RML), and the right lower lobe (RLL).The lobar architecture of the left lung is slightly different because of the location of the heart. There are only two lobes on the left; left upper lobes (LUL) and left lower lobes (LLL) (figure A.1).

Air which is drawn in through the nose or mouth and into the lungs through the trachea. The trachea is a pipe shaped by rings of cartilage. It divides into two tubes called bronchi, which supply air to each lung.

The essential tissue of the lung is called lung parenchyma which is made up of airways, vessels and small air sacs. Inside the lung, the bronchi divide into smaller and smaller tubes called bronchioles. At the end of each of these bronchioles are small air sacs called alveoli (figure A.1). The alveoli are the basic units of the pulmonary system and the area in which gas exchange takes place. Capillaries, which are small blood vessels with thin walls, are wrapped around these alveoli. The walls are so thin and close to each other that the air easily seeps through. In this way, oxygen seeps through into the bloodstream and carbon dioxide, in the bloodstream, seeps through into the alveoli, and is then removed from the

body when we breathe out.

A.1 Lung Tissue Abnormalities

A.1.1 Emphysema

Emphysema is a condition in which the walls between the alveoli or air sacs within the lung lose their ability to stretch and recoil. The air sacs become weakened and break. Elasticity of the lung tissue is lost, causing air to be trapped in the air sacs and impairing the exchange of oxygen and carbon dioxide. Also, the support of the airways is lost, allowing for airflow obstruction. Since emphysema is an interstitial lung disease, it affects the density of the pixels in lung region so the emphysematous regions in the images appear darker (with lower density) [2].

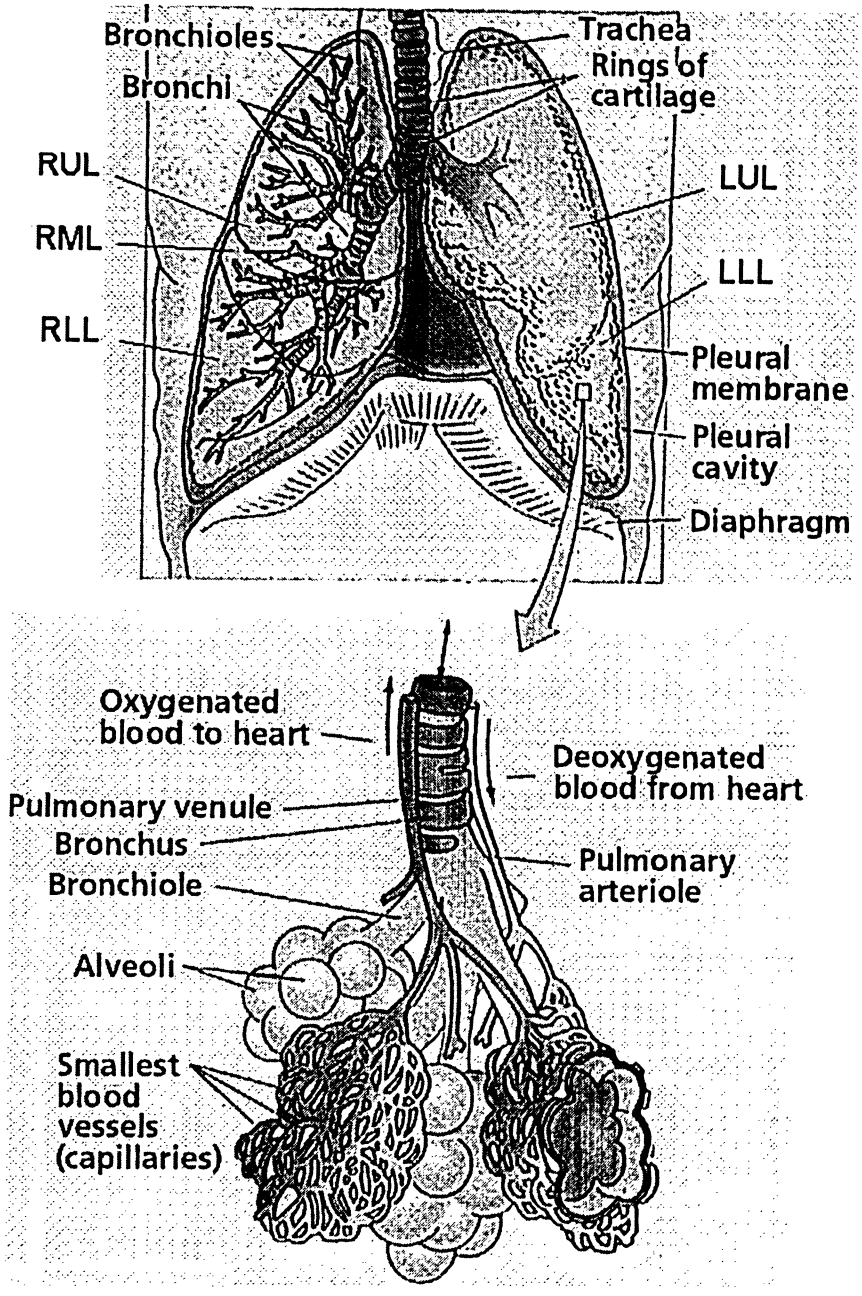

Figure A.1: Lung and its Parenchyma [1].

Appendix B

Fundamentals of Computed Tomography

Computed Tomography (CT) imaging, also known as "CAT scanning" (Computed Axial Tomography), was invented in 1972 by British engineer Godfrey Hounsfield of EMI Laboratories, England. Tomography is from the Greek word "tomos" meaning "slice" or "section" and graphia meaning, "describing". CT is fast, patient friendly and has the unique ability to image a combination of soft tissue, bone, and blood vessels. CT is the imaging system in most busy radiology departments and diagnostic centers. Since its invention, CT imaging has seen massive advances in technology and clinical performance. Today CT enables the diagnosis of a wider array of illness and injury than ever before.

The first CT scanner took several hours to acquire the raw data for a single scan or "slice" and took days to reconstruct a single image from this raw data. The latest of multi-slice CT systems which is believed to be the fastest CT scanner (the Aquilion by Toshiba America Medical Systems figure B.1) rotates around the entire body in half a second. So the exams that once required 30 minutes are now completed in as little as 10 seconds.

Computed Tomography is based on the x-ray principal. A CT scanner looks like a big, square doughnut. The patient aperture (opening) is 60 cm to 70 cm (24" to 28") in diameter. Inside the covers of the CT scanner is a rotating frame, which has an x-ray tube mounted on one side and the banana shaped detector mounted on the opposite side as shown in figure B.2. A fan beam of x-ray is created as the rotating frame spins the x-ray tube and

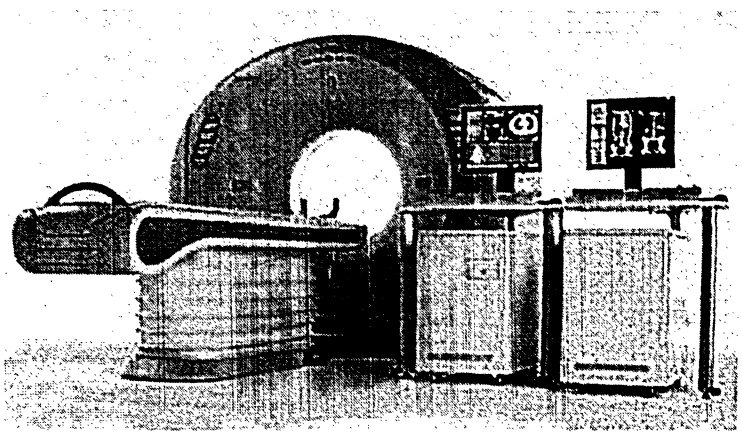

Figure B.1: A Modern CT scanner (Extracted from Aquilion64 User's Guide.

detector around the patient. Each time the x-ray tube and detector make a 360 rotation, an image or "slice" has been acquired. When x-rays pass through the body they are absorbed or attenuated (weakened) at differing levels creating a matrix or profile of x-ray beams of different strength.

This x-ray profile is detected by a banana shaped detector, which measures the x-ray profile. As the x-ray tube and detector make this 360 rotation, the detector takes numerous snapshots (called profiles) of the attenuated x-ray beam. Typically, in one 360 lap, about 1,000 profiles are sampled. Each profile is subdivided spatially (divided into partitions) by the detectors and fed into hundreds of individual channels. Each profile is then backwards reconstructed (or "back projected") into a two-dimensional image of the "slice" by a dedicated computer. The profiles are approximated with Radon Transform of a line which shows the attenuated x-ray beam. Inverse radon transform is used to reconstruct the two dimensional image. In fact each CT image is composed of an abundance of lines. This procedure repeats for each slice to obtain a multislice cross sectional dataset. A modern CT scanner (Aquilion by Toshiba America Medical Systems figure B.1) is capable of producing images 0.5 mm in thickness (distance between the slices), providing more detailed pictures of the body's interior than traditional CTs. With this device exams that once required 30 minutes

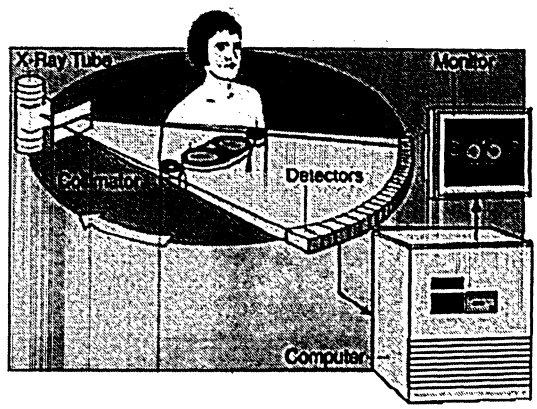

Figure B.2: Fundamentals of a CT scanner (Extracted from Imaginis the Breast Cancer Resource).

are completed in as little as 10 seconds.

B.1 Helical/Spiral Computed Tomography

Computed body tomography has been revolutionized by the technical advantages of Helical/spiral CT (HCT). CT applications are improved by the minimization of motion artifacts and the production of overlapping images without additional radiation exposure.
Helical/Spiral CT scanning involves continuous data acquisition throughout the volume of interest by simultaneously moving the patient through the gantry while the x-ray source rotates [3]. The x-ray traces a spiral on the patients's surface resulting in a helix of raw projection data from which planar images are generated (figure B.3)

Each rotation of the tube generates data specific to an angled plane of section. In order to achieve a true transaxial image, data points above and below the desired plane of section must be interpolated to estimate the data value in the transaxial plane (figure B.4)

Unlike conventional CT, the interval (spacing) between reconstructed transaxial images can be chosen retrospectively and arbitrarily. Thus, overlapping images can be generated without an increase in radiation exposure. So long as raw images data is stored in computer

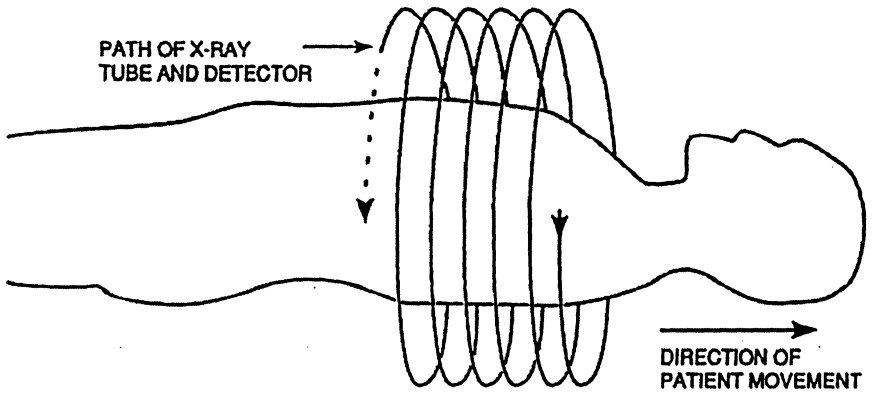

Figure B.3: Schematic drawing of the spiral CT [3].

memory, transaxial images can be generated with as wide or narrow a reconstruction spacing as desired.

B.1.1 Hounsfield Unit

A standardized and accepted unit for reporting and displaying reconstructed X-ray computed tomography CT values is Hounsfield Unit. The system of units represents a linear transformation from the original linear attenuation coefficient measurements into one where water is assigned a value of zero and air is assigned a value of -1000. If w, a, and μ are the linear attenuation coefficients of water, air and a substance of interest, the CT number of the substance of interest is:

$$H = \frac{1000(\mu - w)}{w - a} \tag{B.1}$$

Thus, a change of one Hounsfield unit (HU) corresponds to 0.1% of the attenuation coefficient difference between water and air, or approximately 0.1% of the attenuation coefficient of water since the attenuation coefficient of air is nearly zero. Using this standardized scale facilitates the intercomparison of CT values obtained from different CT scanners and with different X-ray beams energy spectra, although the CT number of materials whose atomic

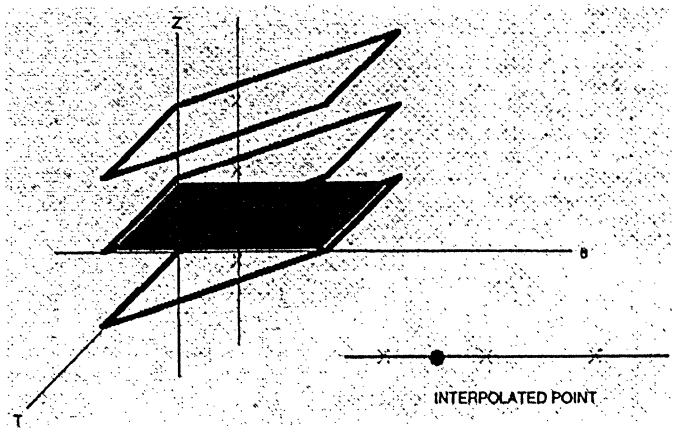

Figure B.4: Schematic of interpolation rationale for helical CT [3].

composition is very different from that of water will be energy dependent.

B.1.2 Digital Imaging and Communications in Medicine (DICOM) Standard

The DICOM Standards are created and maintained for the communication of biomedical, diagnostic and therapeutic information in the medical disciplines that are using digital images and associated data. DICOM is a cooperative standard and its goal is to achieve compatibility and improve workflow efficiency between imaging systems and other information systems in health care environments worldwide. Every major diagnostic medical-imaging vendor in the world has incorporated the standard into its product design, and most are actively participating in the enhancement of the standard. Most biomedical professional societies throughout the world support and participate in the enhancement of this standard. The metadata in a DICOM file provides information, such as the size, dimensions, and bit depth of the image. In addition, the DICOM specification defines a number of other metadata fields that describe many other characteristics of the data, such as the modality used to create the data, the equipment settings used to capture the image, and information about the study.

Bibliography

[1] W. K. Purves, D. Sadava, C. Heller, and G. H. Orians, *"Life: The Science of Biology"*, Sinauer Associates, Inc., 7th edition, December 2003.

[2] W. R. Webb, N. L. Muller, and D. P. Naidich, *"High-Resolution CT of the Lung"*, Lippincott Williams & Wilkins, Univ. of California, San Francisco, 3rd edition, January 2001.

[3] R. K. Zeman, J. A. Brink, P. Costello, W. J. Davros, B. J. Richmond, P. M. Silverman, and P. T. Vieco, *"Helical/Spiral CT, A Practical Approach"*, McGraw-Hill, Inc. Health Professional Division, 1995.

[4] S. G. Armato III, "Cad dissects growing volume of data from lung ct exams," *Diagnostic Imaging Online*, pp. 6–12, November 2003.

[5] R. C. Gonzalez and R. E. Woods, *"Digital Image Processing"*, Prentice Hall Publishing Company, NJ, 2002.

[6] A. Rosenfeld and A. Kak, *"Digital Picture Processing"*, Academic Press, 1982.

[7] M. Levine, *"Vision in Man and Machine"*, McGraw-Hill, 1985.

[8] M. S. Brown, M. F. McNitt-Gray, N. J. Mankovich, J. G. Goldin, J. Hiller, L. S. Wilson, and D. R. Aberle, "Method for segmenting chest ct image data using an anatomical model: Preliminary results," *IEEE Transactions on Medical Imaging*, vol. 16, no. 6, pp. 828–839, December 1997.

[9] H. P. Nii, "Blackboard systems: The blackboard model of problem solving and the evolution of blackboard architectures," *Artificial Intelligence (AI) Magazine*, vol. 7, no. 2, pp. 38–53, 1986.

[10] S. Hu, E. A. Hoffman, and J. M. Reinhardt, "Automatic lung segmentation for accurate quantitation of volumetric x-ray ct images," *IEEE Transactions on Medical Imaging*, vol. 20, no. 6, pp. 490–498, June 2001.

[11] M. Sonka, V. Hlavac, and R. Boyle, *"Image Processing, Analysis and Machine Vision"*, Pacific Grove, CA, 1999.

[12] J. M. Reinhardt and W. E. Higgins, "Paradigm for shape-based image analysis," *Optical Engineering*, vol. 37, no. 2, pp. 570–581, February 1998.

[13] Y. Masutani, K. Masamune, and T. Dohi, "Region-growing based feature extraction algorithm for tree-like objects," *Lecture Notes in Computer Science, K. H. Hhne and R. Kikinis, Eds.*, vol. 1131, 1996.

[14] M.L. Giger, K.T. Bae, and H. MacMahon, "Computerized detection of pulmonary nodules in computed tomography images," *Investigative Radiology*, vol. 29, pp. 459–465, 1994.

[15] C.J. Moran J.T. Blackburn K. Doi H. MacMahon S.G. Armato III, M.L. Giger, "Computerized detection of pulmonary nodules on ct scans," *RadioGraphics*, vol. 19, pp. 1303–1311, 1999.

[16] H. MacMahon S.G. Armato III, M.L. Giger, "Automated detection of lung nodules in ct scans: preliminary results," *Medical Physics*, vol. 28, pp. 1552–1561, 2001.

[17] R.M. Rogers F.C. Sciurba A. Perez B.E. Chapman S. Patel C.R. Fuhrman D. Gur J.K. Leader, B. Zheng, "Automated lung segmentation in x-ray computed tomography: Development and evaluation of a heuristic threshold-based scheme," *Academic Radiology*, vol. 10, pp. 1224–1236, 2003.

[18] R. Haralick, "Statistical and structural approaches to texture," IEEE, May 1979, vol. 67, pp. 786–803.

[19] J. Serra82, *Image Analysis and Mathematical Morphology*, Academic Press, 1982.

[20] Y. Chen and E. Dougherty, "Grey-scale morphological granulometric texture classification," *Optical Engineering*, vol. 33, no. 8, pp. 2713–2722, 1994.

[21] J. Weszka, C. Deya, and A. Rosenfeld, "A comparative study of texture measures for terrain classification," *IEEE Transactions on System, Man and Cybernetics*, vol. 6, pp. 269–285, 1976.

[22] B. Julesz, "Experiments in the visual perception of texture," *Scientific American*, vol. 232, no. 4, pp. 34–43, 1975.

[23] H. Niemann, *Pattern Analysis*, Springer-Verlag, 1981.

[24] R. Lerski, K. Straughan, L. Shad, D. Boyce, S. Bluml, and I. Zuna, "MR image texture analysis an approach to tissue characterisation," *Magnetic Resonance Imaging*, vol. 11, pp. 873–887, 1993.

[25] K. Valkealathi and E. Oja, "Reduced multidimensional co-occurrence histograms in texture classification," *IEEE Transactions on Pattern Analysis and Machine Intelligence*, vol. 20, no. 1, pp. 90–94, 1998.

[26] G. Cross and A. Jain, "Markov random field texture models," *IEEE Transactions on Pattern Analysis and Machine Intelligence*, vol. 5, no. 1, pp. 25–39, 1983.

[27] A. Pentland, "Fractal-based description of natural scenes," *IEEE Transactions on Pattern Analysis and Machine Intelligence*, vol. 6, no. 6, pp. 661–674, 1984.

[28] R. Chellappa and S. Chatterjee, "Classification of textures using gaussian markov random fields," *IEEE Transactions on Acoustic, Speech and Signal Processing*, vol. 33, no. 4, pp. 959–963, 1985.

[29] H. Derin and H. Elliot, "Modeling and segmentation of noisy and textured images using gibbs random fields," *IEEE Transactions on Pattern Analysis and Machine Intelligence*, vol. 9, no. 1, pp. 39–55, 1987.

[30] B. Manjunath and R. Chellappa, "Unsupervised texture segmentation using markov random fields," *IEEE Transactions on Pattern Analysis and Machine Intelligence*, vol. 13, no. 5, pp. 478–482, 1991.

[31] B. Chaudhuri and N. Sarkar, "Texture segmentation using fractal dimension," *IEEE Transactions on Pattern Analysis and Machine Intelligence*, vol. 17, no. 1, pp. 72–77, 1995.

[32] L. Kaplan and C-C. Kuo, "Texture roughness analysis and synthesis via extended self-similar (ess) model," *IEEE Transactions on Pattern Analysis and Machine Intelligence*, vol. 17, no. 11, pp. 1043–1056, 1995.

[33] A. Rosenfeld and J. Weszka, *Digital Pattern Recognition*, chapter Picture Recognition, pp. 135–166, Springer-Verlag, 1980.

[34] J. Daugman, "Uncertainty relation for resolution in space, spatial frequency and orientation optimised by two-dimensional visual cortical filters," *Journal of the Optical Society of America*, vol. 2, pp. 1160–1169, 1985.

[35] A. Bovik, M. Clark, and W. Giesler, "Multichannel texture analysis using localised spatial filters," *IEEE Transactions on Pattern Analysis and Machine Intelligence*, vol. 12, pp. 55–73, 1990.

[36] S.G. Mallat, "A theory of multirresolution signal decomposition: The wavelet representation," *IEEE Transactions Pattern Analysis and Machine Intelligence*, vol. 11, no. 7, pp. 674–693, 1989.

[37] A. Laine and J. Fan, "Texture classification by wavelet packet signatures," *IEEE*

Transactons on Pattern Analysis and Machine Intelligence, vol. 15, no. 11, pp. 1186–1191, 1993.

[38] C. Lu, P. Chung, and C. Chen, "Unsupervised texture segmentation via wavelet transform," *Pattern Recognition*, vol. 30, no. 5, pp. 729–742, 1997.

[39] M. Brady and Z-Y. Xie, *Advances in Image Understanding*, chapter Feature Selection for Texture Segmentation, IEEE Computer Society Press, 1996.

[40] Y. Uchiyama, S. Katsuragawa, H. Abe, J. Shiraishi, F. Li, Q. Li, C. Zhang, K. Suzuki, and K. Doi, "Quantitative computerized analysis of diffuse lung disease in high-resolution computed tomography," *Medical Physics*, vol. 30, no. 9, pp. 2440–2454, September 2003.

[41] K. Doi, "Current status and future potential of computer-aided diagnosis in medical imaging," *British Journal of Radiology*, vol. 78, no. 1, pp. 3–19, January 2005.

[42] A. Fukushima, K. Ashizawa, T. Yamaguchi, N. Matsuyama, H. Hayashi, I. Kida, Y. Imafuku, A. Egawa, and S. Honda S. Kimura, and K. Nagaoki, S. Katsuragawa, K. Doi, and K. Hayashi, "Application of an artificial neural network to high-resolution ct: Usefulness in differential diagnosis of diffuse lung disease," *American Journal of Roentgenology*, vol. 183, pp. 297–305, 2004.

[43] R. Uppaluri, E.A. Hoffman, M. Sonka, P.G. Hartley, G.W Hunninghake, and G. McLennan, "Computer recognition of regional lung disease patterns," *American Journal of Respiratory and Critical Care Medicine*, vol. 160, no. 2, pp. 648–654, August 1999.

[44] R. Uppaluri, T. Mitsa, M. Sonka, E.A. Hoffman, and G. McLennan, "Quantification of pulmonary emphysema from lung computed tomography images," *American Journal of Respiratory and Critical Care Medicine*, vol. 156, no. 1, pp. 248–254, July 1997.

[45] R. Uppaluri, T. Mitsa, and J. R. Galvin, "Fractal analysis of high-resolution ct images

as a tool for quantification of lung disease," in *Medical Imaging*, 1995, vol. 2433, pp. 133–142.

[46] J. Cornelis, J. De Becker, M. Bister, C. Vanhove, G. Demonceau, and A. Cornelis, "Techniques for cardiac image segmentation," in *Engineering in Medicine and Biology Society (EMBS)*, Paris, France, 1992, IEEE, vol. 14, pp. 1906–1908.

[47] S. Buecher and C. Lantuejoul, "Use of watershed in contour detection," in *International Workshop Image Processing, Real-Time Edge and Motion Detection/Estimation*, Rennes, France, September 1979, pp. 17–21.

[48] L. Vincent and P. Soille, "Watersheds in digital spaces: An efficient algorithm based on immersion simulations," *IEEE Transactions on Pattern Analysis and Machine Intelligence*, vol. 13, no. 6, pp. 583–598, June 1991.

[49] V. Grau, A. U. J. Mewes, M. Alcaiz, R. Kikinis, and S.K. Warfield, "Improved watershed transform for medical image segmentation using prior information," *IEEE Transactions on Medical Imaging*, vol. 23, no. 4, pp. 447–458, April 2004.

[50] A. N. Moga and M. Gabbouj, "Parallel marker-based image segmentation with watershed transformation," *Journal of Parallel and Distributed Computing*, vol. 51, no. 1, pp. 27–45, May 1998.

[51] J.B.T.M. Roerdink and A. Meijster, "The watershed transform: Definitions, algorithms and parallelization strategies," *Fundamenta Informaticae*, vol. 41, pp. 187–228, 2001.

[52] S. G. Armato III and W. F. Sensakovic, "Automated lung segmentation for thoracic ct: Impact on computer-aided diagnosis," *Academic Radiology*, vol. 11, no. 9, pp. 1011–1021, September 2004.

[53] L. Vincent, "Morphological grayscale reconstruction in image analysis: Applications and efficient algorithms," *IEEE Transactions on Image Processing*, vol. 2, no. 2, pp. 176–201, April 1993.